

1 **Forest Diversity and Environmental Factors Shape Contrasting** 2 **Soil-Litter Fluxes of Biogenic Volatile Organic Compounds and** 3 **Methane in Three Central Amazonian Ecosystems**

4 Débora Pinheiro-Oliveira^{1*}, Hella van Asperen^{2,3}, Murielli Garcia Caetano⁴, Michelle Robin²,
5 Achim Edtbauer⁵, Nora Zannoni⁶, Joseph Byron⁵, Jonathan Williams⁵, Layon Oreste Demarchi⁷,
6 Maria Teresa Fernandez Piedade⁷, Jochen Schöngart⁷, Florian Wittmann⁸, Sergio Duvoisin-
7 Junior⁹, Carla Batista⁹, Rodrigo Augusto Ferreira de Souza¹⁰, Eliane Gomes Alves^{2,1*}

8 ¹ Graduate Program in Climate and Environment, National Institute for Amazonian Research, Manaus, Brazil

9 ² Department of Biogeochemical Processes, Max Planck Institute for Biogeochemistry, Jena, Germany

10 ³ Institute for Environmental Physics, University of Bremen, Bremen, Germany

11 ⁴ Graduate Program in Tropical Forest Sciences, National Institute for Amazonian Research, Manaus, Brazil

12 ⁵ Atmospheric Chemistry Department, Max Planck Institute for Chemistry, Mainz, Germany

13 ⁶ Institute of Atmospheric Sciences and Climate, National Research Council (CNR-ISAC), Bologna, Italy

14 ⁷ Coordination of Environmental Dynamics, National Institute of Amazonian Research, Manaus, Brazil

15 ⁸ Department of Wetland Ecology, Karlsruhe Institute of Technology, Rastatt, Germany

16 ⁹ Department of Chemistry, Amazonas State University, Manaus, Brazil

17 ¹⁰ Department of Meteorology, Amazonas State University, Manaus, Brazil

18 **Correspondence to:* Débora Pinheiro Oliveira (dpinheiro@bgc-jena.mpg.de); Eliane Gomes Alves ([egomes@bgc-](mailto:egomes@bgc-jena.mpg.de)
19 [jena.mpg.de](mailto:egomes@bgc-jena.mpg.de))

20 **Abstract**

21 Biogenic volatile organic compounds (BVOCs) play a crucial role in biosphere-atmosphere
22 interactions and the global carbon cycle. While vegetation is recognized as the primary source of
23 BVOC fluxes in forest ecosystems, recent studies suggest that the carbon-rich soil-litter
24 compartment plays a significant role in gas fluxes. However, the drivers, variability, and
25 magnitude of these fluxes across different forest types remain poorly understood. This is
26 particularly notable in the Amazon rainforest, the world's largest source of BVOCs, where
27 measurements remain scarce. In this study, we investigated the net soil-litter gas exchange of
28 BVOCs and methane, along with their potential drivers - soil and litter nutrient content, soil and
29 litter microbial biomass, soil temperature, and soil moisture - across three forest types in central
30 Amazonia: White Sand Forest (WS), Upland Forest (Up), and Ancient River Terrace Forest

31 (AR). Our results showed distinct soil-litter gas exchange patterns across the forest types. WS
32 exhibited both high emissions and consumption of gases, notably high acetaldehyde and methane
33 emissions, along with an uptake of monoterpenes. Up showed lower overall fluxes, with
34 moderate emissions and consumption of dimethyl sulfide (DMS), isoprene, and acetaldehyde. In
35 contrast, AR presented no significant fluxes. Among the variables tested, models indicated that
36 soil moisture and temperature were the strongest drivers of fluxes in WS, whereas microbial
37 biomass was the main driver in Up. Our measurements suggest that, despite covering a relatively
38 small area in the Amazon basin, WS can be a significant ecosystem for BVOC and methane
39 fluxes, where these fluxes are influenced by soil moisture and temperature. Our findings
40 underscore the need to account for forest-type-specific fluxes when modeling BVOC and
41 methane emissions in the Amazon, particularly under changing climate conditions.

42 **Key words**

43 Amazon rainforest; Biogenic Volatile Organic Compounds (BVOC); Methane (CH₄); rain-
44 induced emissions; Soil-litter fluxes; Forest heterogeneity; Soil-litter microorganisms

45 **1. Introduction**

46 Biogenic Volatile Organic Compounds (BVOCs) play critical roles across scales, from
47 cellular processes to global climate regulation. While primarily emitted by plants, BVOCs can
48 also be produced and consumed by soil, litter, and microorganisms. Once released into the
49 atmosphere, they actively participate in atmospheric chemistry and physics, influencing climate
50 dynamics. BVOCs react with key atmospheric oxidants - including hydroxyl radicals (OH),
51 ozone (O₃), and nitrate radicals (NO₃) - to form secondary organic aerosols (SOAs) (Artaxo et
52 al., 2022; Yáñez-Serrano et al., 2020). SOAs, in turn, have a major influence on cloud properties,
53 enhancing cloud condensation nuclei (CCN) concentrations, thereby impacting precipitation
54 patterns and altering cloud lifecycles (Liu and Matsui, 2022). Depending on their chemical
55 composition, SOAs can also influence the Earth's radiation budget by scattering incoming solar
56 radiation (resulting in a cooling effect) or absorbing outgoing longwave radiation. Additionally,
57 depending on the concentration of nitrogen oxides (NO_x), BVOCs contribute to the formation of
58 tropospheric ozone - an important greenhouse gas and a major air pollutant (Vella et al., 2025).
59 Given these large-scale impacts, accurately quantifying BVOC fluxes in terrestrial ecosystems is

60 essential for advancing our understanding of forest–atmosphere interactions and for improving
61 Earth system models, thereby improving climate predictions.

62 Global emissions of BVOCs from terrestrial vegetation are estimated at approximately
63 760 Tg C yr⁻¹, with isoprene (C₅H₈) and monoterpenes (C₁₀H₁₆) accounting for around 70% and
64 11% of these emissions, respectively (Guenther et al., 2012; Sindelarova et al., 2014). Isoprene is
65 a simple building block compound emitted in large quantities, particularly by tropical forests.
66 Monoterpenes (e.g., α-pinene, β-pinene, limonene) are structurally more complex (Guenther et
67 al., 2012; Alves et al., 2016), with (-) α-pinene being the second most emitted compound
68 (Zannoni et al., 2020; Yanez-Serrano et al., 2018). The Amazon rainforest alone contributes
69 about 40% of global BVOC emissions, playing a critical role in the global carbon cycle
70 (Guenther et al., 2012; Wang et al., 2024; Tripathi et al., 2025). However, these global estimates
71 primarily consider emissions from plants, neglecting potential contributions from soil and litter,
72 which might also include a large variety of BVOC chemical species. This gap is particularly
73 significant given recent evidence that the soil–litter together is a compartment that can also play
74 a crucial role in BVOC emissions (Bourtsoukidis et al., 2018; Drewer et al., 2021; Fan et al.,
75 2020, 2024; Peñuelas et al., 2014; Tang et al., 2019). Within this compartment, multiple
76 biological and physical processes influence BVOC dynamics. These include plant-related
77 processes such as intra- and inter-organism communication, herbivore defense, and symbiotic
78 interactions (Gfeller et al., 2013; Lin et al., 2007; Rasheed et al., 2021; Steeghs et al., 2004; Tang
79 et al., 2019; Trowbridge et al., 2020). Additionally, soil microorganisms produce and consume
80 BVOCs for communication and ecological interactions (e.g., defense and competition), with
81 these compounds also being released as residual metabolic products (Isidorov & Jdanova, 2002;
82 Leff & Fierer, 2008; Liu et al., 2024; Monard et al., 2021; Crocker et al., 2025).

83 Greenhouse gases (GHGs), such as methane (CH₄), carbon dioxide (CO₂), and nitrous
84 oxide (N₂O), are also produced and consumed by soil microorganisms through key metabolic
85 processes, including methanogenesis, methanotrophy, and microbial respiration (Conrad,
86 2009,2020; Hofmann et al., 2016). While CO₂ and methane are not classified as BVOCs, they
87 play a crucial role in overall gas exchange processes and provide a broader perspective of soil-
88 litter gas (carbon) fluxes. Moreover, environmental factors such as soil moisture, temperature,
89 and nutrient availability influence both BVOC and GHG fluxes, albeit through distinct but

90 interconnected biological and physical mechanisms (Greenberg et al., 2012; Tang et al., 2019;
91 Asensio et al., 2007). These interconnected processes drive net ecosystem gas exchange between
92 the soil-litter compartment and the atmosphere, making methane and CO₂ key components for
93 understanding processes driving BVOC flux dynamics.

94 Fluxes of GHGs and BVOCs can also be linked to litter decomposition. This process is
95 influenced by various physical factors, including soil moisture, temperature, and nutrient
96 availability, which collectively can enhance microbial activity—one of the main drivers of these
97 fluxes (Greenberg et al., 2012; Tang et al., 2019; Mäki et al., 2017; Asensio et al., 2007).
98 Specifically, microbial processes such as nitrification and denitrification can result in the
99 production and consumption of N₂O in soils (Butterbach-Bahl et al., 2013; Snyder et al., 2009).
100 Together, these processes drive the net ecosystem exchange of BVOCs and GHGs between the
101 soil-litter compartment and the atmosphere, and the magnitude and direction of this exchange
102 may vary across different ecosystem types.

103 The Amazon Basin is a mosaic of diverse forest types (Oliveira-Filho et al., 2021), each
104 with distinct plant species composition (Ter Steege et al., 2013), shaped by the region's highly
105 variable soil properties (Quesada et al., 2011; Quesada et al., 2012). Although Amazonian
106 heterogeneity is known to play a critical role in regulating biogeochemical cycles, comparative
107 studies across forest types, especially at the soil–litter interface, are still scarce. Distinct
108 interactions between vegetation and soil can lead to highly variable patterns of BVOC and GHG
109 exchange. This lack of representation underscores the urgent need for studies that account for the
110 region's ecological diversity to capture better the unique contributions of each forest type to
111 biogeochemical processes. Quantifying this variability is key to improving both regional and
112 global models, as gas fluxes are unlikely to be uniform within the Amazon.

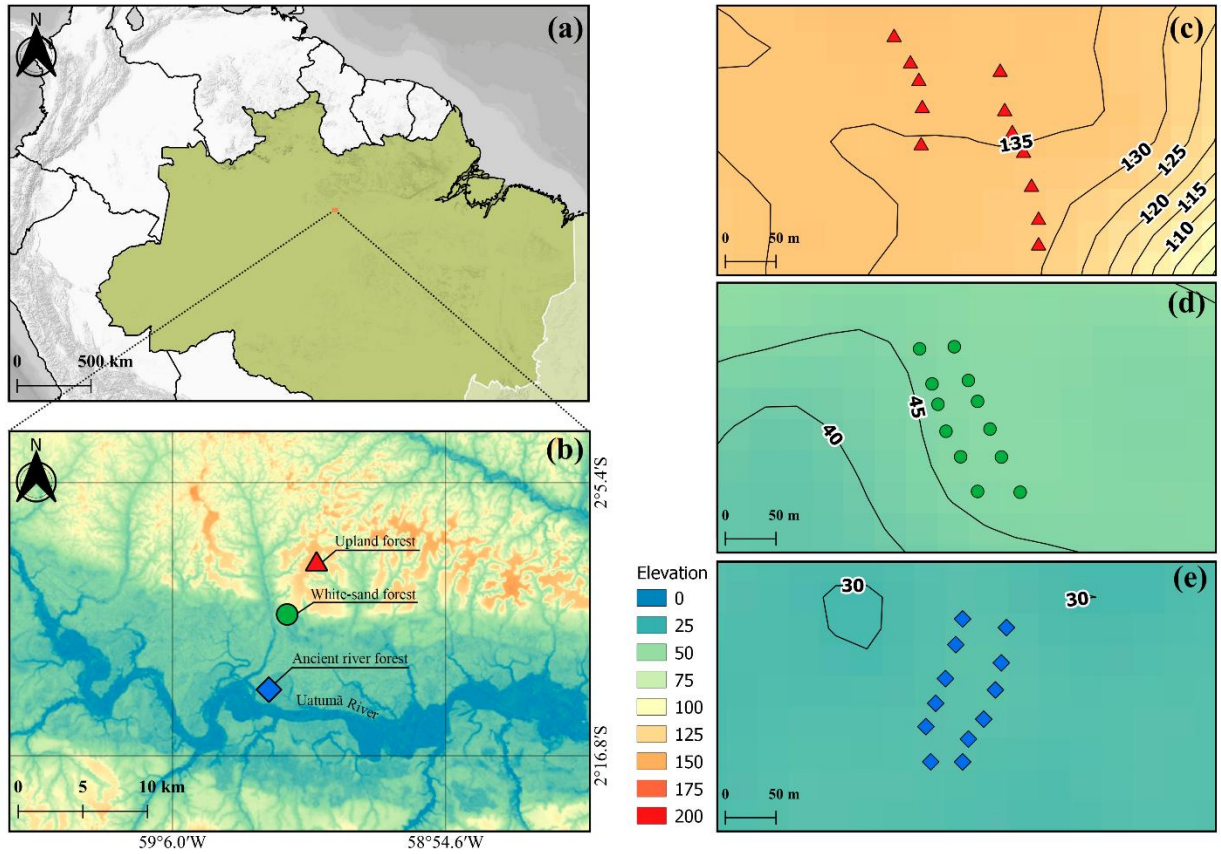
113 To address these gaps, we investigated soil-litter fluxes of BVOCs (acetaldehyde,
114 methanol, m/z 42, dimethyl sulfide, isoprene and monoterpenes) and GHGs (CH₄ and CO₂), soil
115 and litter nutrient content and microbial biomass, and soil temperature and moisture from three
116 forest types in central Amazonia: (i) Ancient River Terrace Forest - a forest that was flooded in
117 the past and is no longer flooded due to changes in the river course (paleoigapó); (ii) White Sand
118 Forest (locally called campinarana) - a less common forest type that occupies about 5% of the

119 Amazon basin (Adeney et al., 2016); and (iii) Upland Forest (locally called terra-firme) - the
120 most common forest in Amazonia, with the highest plant species richness (Emidio et al., 2016;
121 Luize et al., 2018). We aimed to answer the following questions: (i) what is the
122 emission/consumption of BVOCs, CO₂, and CH₄ in magnitude and chemical diversity, and; (ii)
123 what are the main drivers of soil-litter gas exchanges across these three forest types in central
124 Amazonia (specifically, soil moisture, soil temperature, nutrient content and microbial biomass
125 from soil and litter)?

126 **2. Material and Methods**

127 **2.1 Site Description**

128 This study was conducted in the MAUA–PELD experimental plots (PELD is the
129 abbreviation in Portuguese for long-term ecological research) (Fig. 1) at the Amazon Tall Tower
130 Observatory (ATTO) experimental site. This site is located 150 km northeast of Manaus and is
131 part of the Uatumã Sustainable Reserve (USDR), which covers an area of 424,430 hectares
132 (Andreae et al., 2015). The climate is tropical humid, with average annual rainfall of 2,376 mm
133 and a temperature of 28°C (Botía et al., 2022). There are two distinct seasons, the wet season
134 from December to May and the dry season from July to October, with transition seasons in
135 between. The ATTO site contains three dominant non-flooded ecosystems: a dense Upland
136 Forest (Up) on the plateau, with an elevation close to 100 m (*terra-firme*); a White Sand Forest
137 (WS) (*campinarana*); and another type of *terra-firme* vegetation that developed on the lower-
138 laying ancient river terraces (Ancient River Terrace Forests (AR)) (Fig. 1) (Andreae et al., 2015).



139

140 **Figure 1.** (a) Location of the ATTO site. (b) A map illustrating the locations of the different
 141 forest types evaluated in this study: Upland Forest (Up), White Sand Forest (WS), and Ancient
 142 River Terrace Forest (AR), and showing the Uatumã River, a tributary of the Amazon River. (c),
 143 (d) and (e): The distribution of sampling points along the Transects in each forest type (Upland
 144 Forest - top, White Sand Forest - middle, and Ancient River Terrace Forest - bottom); black lines
 145 and numbers indicate the elevation (above sea level – a.s.l.).

146 Topography is critical to soil formation in the central Amazon region (Quesada et al.,
 147 2009). At the ATTO site, a clear topographic gradient is associated with different soil
 148 characteristics (Fig. 1). In the Ancient River Terrace Forest, soil contains more silt and clay
 149 (39% sand, 37% silt, 23% clay) in comparison to the adjacent sandy White Sand Forest soils
 150 (57% sand, 40% silt, 1.50% clay). Upland Forest soils are more clayey and contain very little
 151 sand (13% total sand, 34% silt, 52% clay) (data from this study; supplementary material, Section
 152 1; Table S1). Upland Forest soils, which are predominantly ferrasols, are known to hold more
 153 water than other tropical soils, benefiting forest activity during the dry season (Quesada et al.,

154 2009). Ancient River Terrace Forest soils are typically allisols, younger and richer in nutrients
155 compared to upland ferralsols (Andreae et al., 2015). White Sand Forest soils are arenosols,
156 characterized by high permeability and low water retention, with low specific heat capacity and
157 often nutrient-poor organic layers (Quesada et al., 2011). The study area in the White Sand
158 Forest has high water table variability, with a hard subsoil layer that restricts drainage and can
159 flood the root system during the wet season (Demarchi et al., 2022).

160 **2.2 Sampling Design**

161 For each forest type, a PELD-MAUA plot (~1 hectare) (<https://peld-maua.inpa.gov.br>) was
162 selected. Within each plot, two 150 m Transects were established (Fig. 1) in homogeneous areas
163 characterized by consistent vegetation structure, soil characteristics, and topography, to minimize
164 spatial variability and avoid pseudo-replication. Along each Transect, six sampling points were
165 marked at ~30 m intervals, resulting in a total of 36 soil chamber measurements conducted on
166 consecutive days; although this design was necessary for logistical reasons, it also allowed us to
167 examine the influence of external factors beyond forest-type differences. Chamber-based
168 methods (Section 2.3; Fig. 1) were employed for the in-situ quantification of CO₂, CH₄, and
169 BVOC fluxes from the soil–litter compartment. These chambers were installed directly in the
170 field with minimal disturbance to the surrounding environment. To account for potential
171 background signals and chamber interferences, three blank chambers, with the same dimensions
172 as the sample chamber, but each featuring completely bottom-sealed collars, were deployed per
173 Transect and measured simultaneously alongside the sample chambers (Fig. 2b).

174 Tedlar bags (CEL Scientific, Cerritos, CA, USA) were used to collect gas samples
175 directly from the outlet of the pump connected to the chambers, capturing the air for subsequent
176 analysis of BVOCs, CO₂, and CH₄. After each gas flux measurement, soil temperature (T, °C)
177 (TP-101, Delhi, India) and soil volumetric water content (VWC, %) were measured around the
178 collar five times using a probe (AT SMT150, Cambridge, UK), and the averages were calculated.
179 Surface soil samples were collected from the organic layer, approximately within the upper 5 cm
180 of the soil. Samples from the litter and surface soil layers were collected inside the chamber and
181 stored for analysis of chemical and physical characteristics and microbial biomass. Due to
182 expected low variation and limited possibility for laboratory analyses, nutrient samples from soil

183 and litter (excluding carbon and nitrogen) and granulometry were collected as mixed samples
184 pooled and homogenized from two collars. To minimize diurnal variation, each Transect was
185 measured between 8:00 and 10:00 (local time), after which collected samples were processed and
186 analyzed for BVOC and GHG concentrations. During the measurements, no precipitation was
187 observed, but one large rain event occurred just before the measurement of Transect 2 of the
188 White Sand Forest.

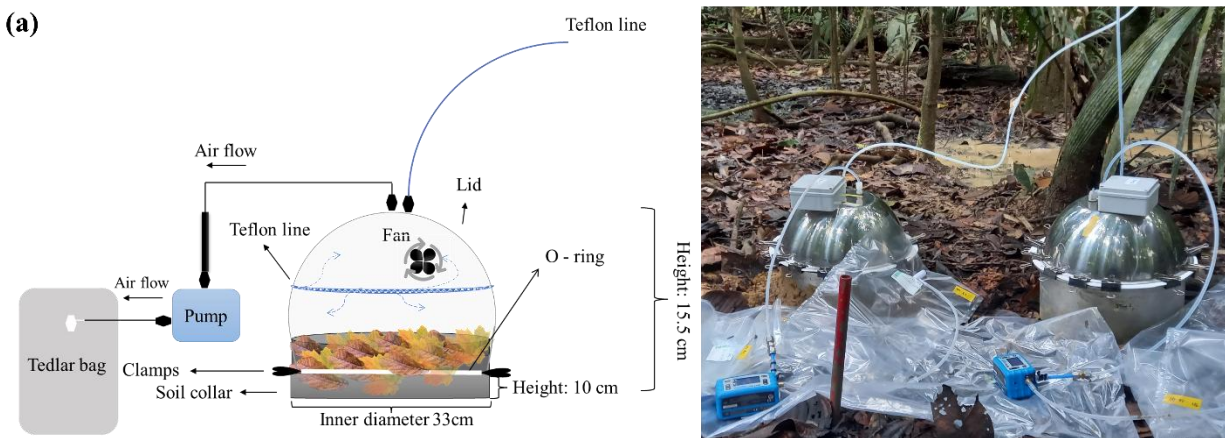
189

190 **2.3 Flux Chamber Measurements**

191

192 The flux chambers used in this study were produced by the Max Planck Institute for
193 Biogeochemistry. The soil chamber, consisting of a lid and a soil collar (Fig. 2a), was made
194 entirely of 100% stainless steel, with a total volume of 21 L and a surface area of 855 cm²
195 (0.0855 m²). The blank chamber collar had the same dimensions as the soil collar but contained a
196 sealed bottom. Two Teflon inlets were connected to the top of the chamber, and inside the
197 chamber was a fan that mixed the gases in the chamber headspace. A PTFE-coated Viton O-ring
198 was positioned at the edge of the collar over which the chamber was placed, ensuring a tight seal
199 between the chamber and the collar.

200 Before gas sampling, each collar was carefully installed in a non-invasive manner by
201 gently pressing its edge into the litter and surface soil to minimize disturbance to plant shoots
202 and roots. To further ensure a tight seal preventing any potential leakage, the surrounding soil
203 was carefully pressed against the outer edges of the collar (Aaltonen et al., 2011). This method
204 ensured that the chamber system was effectively isolated from external gas exchange. The
205 chamber and collar were sealed together with multiple clamps to prevent outside air from
206 entering the chamber during measurements. The collars were installed approximately 24 hours
207 prior to sampling to allow the surrounding environment to stabilize.



208

209 **Figure 2.** (a) Schematic of the flux chamber. (b) Photo of the measurement setup of the
 210 sample and the blank chamber.

211 Gas collection took place in December 2021, during the dry-to-wet season transition.
 212 Before placing the lid on the collar, the chamber was manually ventilated to minimize gas
 213 accumulation caused by the collar. Once the chamber was closed and sealed with clamps, the
 214 internal fan was turned on to ensure mixing. An air sampling pump (GilAir® Plus, Levitt Safety,
 215 Ottawa, ON), operating at a flow rate of 500 sccm, initiated continuous flow from the chamber
 216 outlet immediately after closure to maintain constant conditions throughout the measurement.

217 After 20 minutes of chamber closure with continuous air circulation, a Tedlar bag was
 218 connected to the outlet of the Teflon pump, and a 5 L air sample was collected over the next 10
 219 minutes. By the end of the 30-minute measurement process, a total of 15 L of air had flowed
 220 through the chamber, and the last 5 L were used for subsequent analyses. The sample volumes
 221 collected were determined by the specific requirements of each analytical instrument.
 222 Measurements of BVOCs were performed using proton-transfer-reaction quadrupole mass
 223 spectrometry (PTR-QMS; IONICON Analytik, Innsbruck, Austria), prioritizing sufficient ion
 224 counts per second (CPS) and integration cycles for reliable detection of BVOC concentrations
 225 with the required precision, especially considering their typically trace levels. Greenhouse gases
 226 (GHGs) were measured using a Los Gatos Ultra-Portable Gas Analyzer (California, USA),
 227 hereafter referred to as the Los Gatos analyzer. Finally, for the offline measurements with
 228 cartridges and for specific compound identification and qualitative analysis with thermal-
 229 desorption gas chromatography time-of-flight mass spectrometry (TD-GC-TOF-MS; Bench ToF

230 Tandem Ionisation, Markes International, Bridgend, UK), at least 2 L of sample air was required
231 to effectively load the adsorbent cartridges. These analyses are further detailed in the
232 Supplementary Materials, Section 4.2.

233 The same procedure was followed by a blank chamber, which was measured under
234 identical conditions to account for gas contributions unrelated to soil and litter processes. For
235 logistical reasons, measurements were conducted with three chambers simultaneously, pairing
236 two sample chambers with one blank chamber, followed by two additional sets, resulting in the
237 measurement of six samples and three blank chambers per day. Because air was continuously
238 extracted from the chamber headspace by the pump, ambient air entered the chamber through
239 one additional inlet, which consisted of a 2 m long open Teflon tube, fixed approximately 2 m
240 above the ground and positioned at the same location for both sample and blank chambers. The
241 setup ensured that both chambers (sample and blank) were diluted or affected by ambient air to
242 the same degree, minimizing potential biases.

243 After sampling, bags were handled carefully to prevent leakage. Potential compound
244 losses due to adsorption onto the inner walls or diffusion through the bag material were
245 minimized by storing all samples in a dark, stainless-steel box to avoid light exposure and
246 keeping them in air-conditioned lab containers at low temperatures until analysis. All samples
247 were analyzed on the same day, within a maximum of 8 hours post-collection, following the
248 recommendations of Beauchamp et al. (2008). Gas analysis began with the quantification of
249 BVOCs using a PTR-QMS. Subsequent analyses of CO₂ and CH₄ concentrations were conducted
250 using a Los Gatos analyzer. Each sample bag was then used to fill stainless steel cartridges
251 (containing Tenax TA and Carbograph 5TD adsorbents), which were later analyzed via TD-GC-
252 TOF-MS. Detailed descriptions of the analytical procedures and results are in Sections 4 and 4.1
253 of the Supplementary Material.

254

255 **2.4 PTR-QMS measurements and Los Gatos analyzer measurements**

256 Tedlar bags were connected to the PTR-QMS for analysis of BVOCs (Lindinger et al.,
257 1998). The PTR-QMS H₃O⁺ mode was used for chemical ionization, which is extremely
258 sensitive to all BVOCs that have a higher proton affinity than water, covering most volatile
259 organic compounds (Edtbauer et al., 2021). Six compounds were analyzed (Table 1). The PTR-

260 QMS was operated under standard conditions at 2.3 mbar, and E/N 120, with 60°C, with a drift
 261 tube voltage of 600 V. During each PTR-QMS measurement cycle, the following specific
 262 protonated mass-to-charge ratios (m/z) were measured, 21 (H₃O¹⁸⁺), 32 (O₂⁺), and 37 (H₂O-
 263 H₃O⁺), with a dwell time of 500 ms each; and Methanol (33), compound not identified (m/z 42),
 264 Acetaldehyde (45), Dimethyl sulfide - DMS (63), Isoprene (69) and Monoterpenes (137), with a
 265 dwell time of 1 second. We measured approximately 17 cycles for each bag. Mass identifications
 266 were based on the available literature (Warneke et al., 2015) and were consistent with a PTR-MS
 267 mass library database - GLOVOC (Yañez-Serrano et al., 2021) and gas calibration with certified
 268 standards.

269 **Table 1.** Compounds analyzed by the PTR-QMS

BVOC	Chemical formula (H ⁺)	m/z	Group	270
Methanol	CH ₄ O ⁺	33	Alcohol	271
not identified		42	N-compound	272
Acetaldehyde	C ₂ H ₄ O ⁺	45	Aldehyde	273
Isoprene	C ₅ H ₈ ⁺	69	Alkenes	
Dimethyl sulfide (DMS)	C ₂ H ₆ S ⁺	63	Organosulfides	274
Monoterpenes	C ₁₅ H ₁₆ ⁺	137	Alkenes	275

276 Calibrations were performed before the experiment using a multi-component calibration
 277 mix containing various gases of known concentrations (Apel-Riemer Environmental, Inc.)
 278 (supplementary material; Section 2; Table S2). Four-point calibration curves were generated by
 279 diluting the multicomponent with synthetic air, humidifying the air stream with a water bubbler
 280 filled with distilled water, and controlling the flow with mass flow controllers (supplementary
 281 material; Section 2; Fig. S1). Curves were calculated considering the normalized counts per
 282 second as a function of the mixing ratio. Previously, some compounds important for soil-litter
 283 processes (Peñuelas et al., 2014) - such as acetone, ethanol, and formaldehyde - were considered
 284 for this study, but as they did not show a good fit, they were excluded from this work. The error
 285 of PTR-QMS concentration measurements of the six presented compounds is expected to consist
 286 of a systematic part and a statistical part. The systematic error consists of the uncertainty of the
 287 calibration gas standard (+5%), the error of the flow measurements (+5%), and the error of the
 288 calibration slope (14.8%, 52.4%, 12.5%, 18.4%, 18.2% for methanol, m/z42, acetaldehyde, DMS

289 and monoterpenes, respectively). The statistical error is based on the repeatability of the
290 concentration measurement during the calibration routine, and was found to be 14.4%, 26.2%,
291 14.8%, 13.7%, 6.0% for methanol, m/z42, acetaldehyde, DMS and monoterpenes, respectively.
292 The systematic error affects both bags in the same direction, whereas the statistical error can
293 differ between the two bags in a pair. Therefore, to evaluate the uncertainty of the fluxes, we
294 focused on the propagated statistical uncertainty, as described in Section 2.5.

295 After PTR-QMS analysis, the bags were connected to a Los Gatos analyzer to measure
296 the mixing ratios of methane and CO₂. The Los Gatos analyzer is an instrument based on laser
297 absorption spectroscopy, specifically Off-axis Integrated Cavity Output Spectroscopy (OA-
298 ICOS), enabling ultra-sensitive, precise, and real-time measurements of trace gases in gas
299 samples (Pohlman et al., 2021; van Asperen et al., 2024). The instrument operates at a relatively
300 low sample flow rate (~ 0.1 L min⁻¹), and a minimum gas volume of 0.3 L was used as a
301 precaution to ensure measurement stability and accurate determination of CH₄ and CO₂
302 concentrations; air from the sample bags was analyzed for 3 minutes, and mean concentrations
303 were calculated from the final 2 minutes of measurement.

304 **2.5 BVOC & GHG flux calculation**

305 To calculate BVOC and GHG fluxes, the Volumetric Mixing Ratios of the blank chamber
306 bags (VMR_b) were subtracted from the sample chamber bags (VMR):

$$307 \quad dVMR = VMR - VMR_b \quad (1)$$

308 In which VMR is expressed in pptv or ppbv. By subtracting the mixing ratios of a blank
309 chamber, dVMR represents the concentration difference attributable solely to soil and litter
310 fluxes, corrected for potential chamber effects or the influence of ambient air entering the
311 system. To ensure data reliability, bag pairs for which the concentration difference (dVMR) was
312 less than or equal to the combined statistical uncertainty (calculated using the Root-Sum-Square
313 method from the individual bag uncertainties) were assigned a value of zero. This approach
314 ensures that only reliably detected fluxes are considered while retaining the full sample size for
315 modeling. For simplicity, we used a closed chamber approach to calculate fluxes rather than the
316 open steady-state approach. The constant sample flow introduces a dilution effect that may lead
317 to an underestimation of the fluxes by up to 25% (see Supplementary Material, Section 3). The

318 reported fluxes should therefore be considered conservative estimates, and this potential bias
319 does not affect the main conclusions of the study.

320 To convert dVMR to fluxes, we used:

$$321 \quad F = dVMR * N * (V / A) * (1/T) \quad (2)$$

322 where N is the value of fixed molar volume at 25 °C (24.8 L mol⁻¹; 40.3 mol m⁻³), V is the
323 chamber volume (0.021 m³), A is the chamber area (0.0855 m²), and T is the average sampling
324 time (25 min). Flux values in nmol m⁻² min⁻¹ were converted to ng m⁻² h⁻¹.

325 **2.6 Soil and Litter Analyses**

326 The Thematic Laboratory of Soils and Plants (LTSP, at the National Institute for
327 Amazonian Research - INPA) analyzed soil and litter nutrient content according to adapted
328 protocols (EMBRAPA, 1999). The nutrients - iron (Fe⁺²), calcium (Ca⁺²), magnesium (Mg⁺²),
329 zinc (Zn⁺²), potassium (K⁺), manganese (Mn⁺), phosphorus (P), and aluminum (Al) - were
330 determined by digestion with a nitro-perchloric acid solution (Malavolta et al., 1989). Total
331 phosphorus (P) was quantified using colorimetry (Murphy & Riley, 1962; Olsen & Sommers,
332 1982) and measured using a UV spectrophotometer (Model 1240, Shimadzu, Kyoto, Japan).
333 Potassium (K), calcium (Ca), and magnesium (Mg) concentrations were determined by atomic
334 absorption spectrophotometry (AAS, 1100 B, 250 Perkin Elmer, Ueberlingen, Germany), as
335 described by Anderson and Ingram (1993). Soil carbon and nitrogen content was determined by
336 the Routine Measurements & Analyses Lab (RoMA, MPI-BGC) with the elemental analyzer
337 "varioEL" (Elementar Analysensysteme GmbH, Elementar-Straße 1, D-63505 Langenselbold,
338 Germany). Soil porosity was analyzed using the pycnometer method described in Flint & Flint
339 (2002). The amount of water was corrected for soil density.

340 For analysis of soil and litter microbial Carbon, Nitrogen, and Phosphorus (C, N, and P)
341 contents, 2g of fresh litter and 5g of fresh soil were used from each sample chamber. These were
342 separated into fumigated and non-fumigated samples. The fumigated samples were left with
343 chloroform for 24 hours and then divided into two sub-samples. First, 50 mL of KCl (Potassium
344 Chloride) was added, and total C and N were extracted, and for the second, 50 mL of NaHCO₃
345 (Sodium Bicarbonate) was added for total P extraction. Following the same extraction protocol,
346 the non-fumigated samples were prepared for direct extraction without going through the 24-

347 hour fumigation period. Microbial C, N, and P content was estimated in fumigated and non-
348 fumigated extracts from the difference in organic C, N, and total P measured by a TOC/TN
349 analyzer (Jenkinson et al., 2004). The extraction of the microbial biomass was performed at
350 INPA, and the analyses were done by the Routine Measurements & Analyses Lab (RoMA, MPI-
351 BGC).

352 The litter layer inside the measurement collars was not quantified in terms of litter mass
353 or plant species composition. However, during field sampling, we qualitatively observed spatial
354 variation in litter accumulation among measurement points and forest types, reflecting the
355 natural heterogeneity of litter inputs typical of Amazonian forests. In general, thicker litter layers
356 were observed in the Ancient River Terrace Forest and the White Sand Forest, which appeared
357 broadly similar in litter accumulation, whereas the Upland Forest tended to have comparatively
358 thinner layers.

359

360 **2.7 Statistical analyses**

361 A total of 36 samples were evaluated ($n = 12$ per forest type). Gas fluxes were first
362 correlated with potential predictors (soil and litter characteristics, Table 2), revealing variations
363 between forest types. Separate regression models were built for each forest type to maximize
364 predictive ability, with variable selection based on the following criteria: 1) given the statistical
365 power limitation of models ($n = 12$), the maximum number of independent variables possible to
366 include was two; thus, 2) we tested all models with one or two independent variable
367 combinations; finally, 3) we chose the models which showed no multicollinearity and had the
368 highest adjusted R-squared and lowest Akaike's information criterion (AIC). The
369 "ols_step_all_possible" function from the "olsrr" package (Hebbali, 2024) was used, and
370 multicollinearity was assessed via VIF (<2.5 ; Hair et al., 2009). Principal Component Analysis
371 (PCA) and Pearson's correlation (Hmisc package; Harrell, 2018) were performed to explore
372 variable interactions. Variations within forest types (e.g., between Transects) were analyzed
373 using t-tests for normal data and Kruskal-Wallis tests for non-normal data, with a significance
374 level of 0.05. All analyses were conducted in R (v4.3.0; R Core Team, 2023).

375

376 **Table 2.** Variables, their respective codes, and units.

Variable	Code	Unit
Soil carbon	c_soil	%
Soil nitrogen	n_soil	%
Soil phosphorus	p_soil	P mg/kg
Soil potassium	k_soil	K ⁺ mg/kg
Soil calcium	ca_soil	Ca ⁺² mg/kg
Soil magnesium	mg_soil	Mg ⁺² mg/kg
Soil aluminum	al_soil	Al ⁺³ mg/kg
Soil iron	fe_soil	Fe ⁺² mg/kg
Soil zinc	zn_soil	Zn ⁺² mg/kg
Soil manganese	mn_soil	Mn ⁺² mg/kg
Soil ph	ph_soil	pH
Soil temperature	soil_temp	Celsius
Soil moisture	soil_moisture	%
Litter carbon	c_litter	%
Litter nitrogen	n_litter	%
Litter calcium	ca_litter	Ca ⁺² mg/kg
Litter magnesium	mg_litter	Mg ⁺² mg/kg
Litter potassium	k_litter	K ⁺ mg/kg
Litter iron	fe_litter	Fe ⁺² mg/kg
Litter zinc	zn_litter	Zn ⁺² mg/kg
Litter manganese	mn_litter	Mn ⁺² mg/kg
Microbial biomass soil carbon	c_mic_soil	g/kg
Microbial biomass soil nitrogen	n_mic_soil	g/kg
Microbial biomass soil phosphorus	p_mic_soil	g/kg
Microbial biomass litter carbon	c_mic_litter	g/kg
Microbial biomass litter nitrogen	n_mic_litter	g/kg
Microbial biomass soil phosphorus	p_mic_litter	g/kg

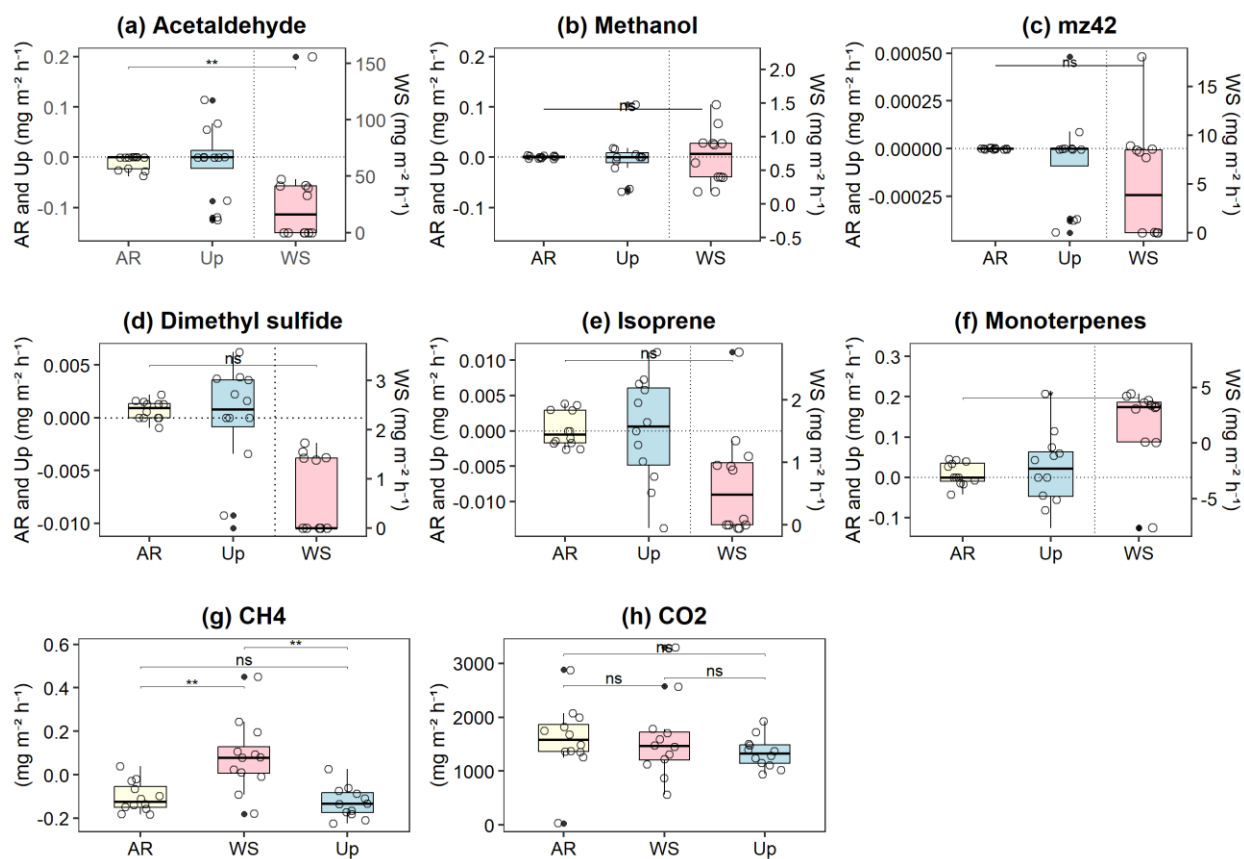
377

378 **3. Results**

379 **3.1 Comparison between forest types**

380 The three forest types showed very different gas fluxes for BVOCs and GHGs (Fig. 3),
 381 with the highest fluxes observed in the White Sand Forest. Fluxes were very low in the Upland
 382 Forest, and almost no gas fluxes were observed in the Ancient River Terrace Forest.
 383 Acetaldehyde emissions showed the most significant differences between forest types, with flux

384 averages of $35.87 \pm 46.86 \text{ mg m}^{-2} \text{ h}^{-1}$ (mean \pm SD) for the White Sand Forest, $-0.09 \pm 0.02 \text{ mg}$
 385 $\text{m}^{-2} \text{ h}^{-1}$ for the Upland Forest, and $-0.02 \pm 0.008 \text{ mg m}^{-2} \text{ h}^{-1}$ for the Ancient River Terrace Forest.
 386 Isoprenoid (isoprene and monoterpenes) fluxes were also high in the White Sand Forest, and
 387 clear differences were found between forest types concerning the speciation of monoterpenes
 388 (supplementary material; Fig. S2).

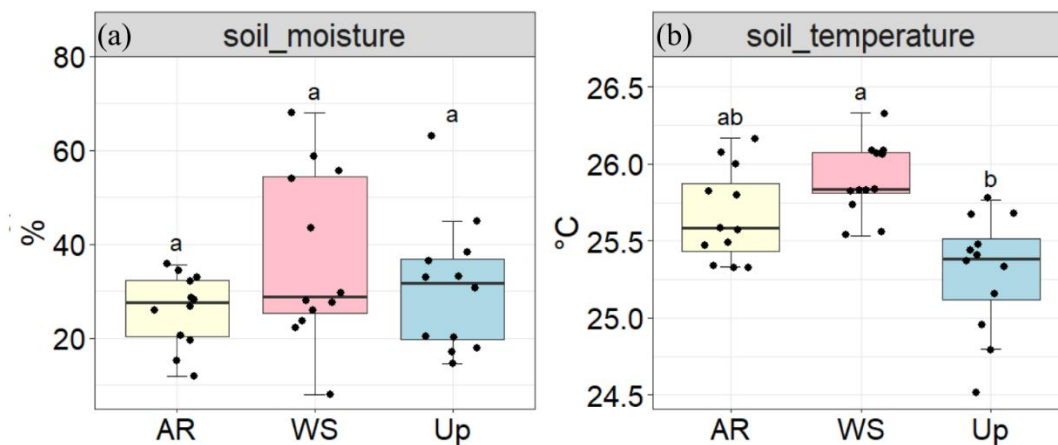


389

390 **Figure 3.** Soil–litter fluxes of biogenic volatile organic compounds (BVOCs) and greenhouse
 391 gases (GHGs) across three forest types: Ancient River Terrace Forest (AR), White Sand Forest
 392 (WS), and Upland Forest (Up). Panels show fluxes of (a) acetaldehyde, (b) methanol, (c) m/z 42,
 393 (d) dimethyl sulfide (DMS), (e) isoprene, (f) monoterpenes, (g) methane (CH₄), and (h) carbon
 394 dioxide (CO₂). Statistical differences between forest types are indicated by horizontal brackets (p
 395 < 0.05 ; $p < 0.01$), while “ns” denotes non-significant differences (N = 36). Differences were
 396 assessed using ANOVA for normally distributed data and the Kruskal–Wallis test for non-
 397 normal data, followed by Dunn’s post hoc test with Bonferroni correction. Boxes represent the

398 median (horizontal line) and the interquartile range (IQR). Whiskers extend to $1.5 \times$ IQR, and
399 points represent individual observations.

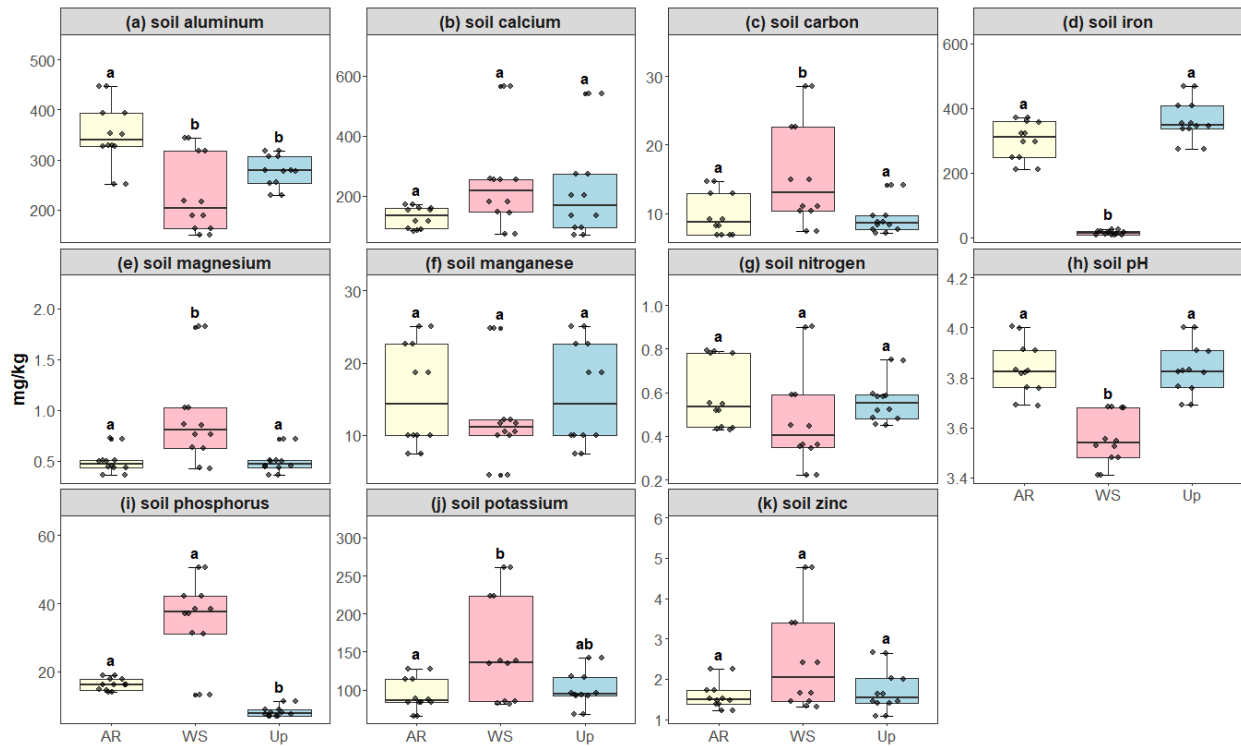
400 In the White Sand Forest, high isoprenoid emissions were observed, with isoprene fluxes
401 averaging $0.66 \pm 0.84 \text{ mg m}^{-2} \text{ h}^{-1}$, and monoterpene fluxes averaging $1.12 \pm 4.31 \text{ mg m}^{-2} \text{ h}^{-1}$.
402 Details on the monoterpene and sesquiterpene speciation can be found in Supplementary
403 Material, Section 4.2. Conversely, very low (negative) values were recorded in the Upland Forest
404 (Isoprene, $-0.005 \pm 0.003 \text{ mg m}^{-2} \text{ h}^{-1}$ and monoterpenes $-0.02 \pm 0.08 \text{ mg m}^{-2} \text{ h}^{-1}$) and Ancient
405 River Terrace Forest (Isoprene, $-0.002 \pm -0.001 \text{ mg m}^{-2} \text{ h}^{-1}$ and monoterpenes -0.011 ± 0.015
406 $\text{mg m}^{-2} \text{ h}^{-1}$). In the WS we also observed the consumption of monoterpenes (with -7.63 mg m^{-2}
407 h^{-1} , highlighted as an outlier in Fig. 3) and high emissions of DMS ($1.10 \pm 1.14 \text{ mg m}^{-2} \text{ h}^{-1}$),
408 whereas a consumption of the latter was observed in the Upland Forest ($-0.001 \pm 0.005 \text{ mg m}^{-2}$
409 h^{-1}) and Ancient River Terrace Forest ($-0.0003 \pm 0.001 \text{ mg m}^{-2} \text{ h}^{-1}$). CH_4 fluxes showed
410 substantial variation in the White Sand Forest, with both uptake ($-0.09 \pm 0.16 \text{ mg m}^{-2} \text{ h}^{-1}$) and
411 emission ($0.08 \pm 0.07 \text{ mg m}^{-2} \text{ h}^{-1}$). In contrast, the Upland Forest and Ancient River Terrace
412 Forest showed methane uptake primarily, with average fluxes of $-0.14 \pm 0.05 \text{ mg m}^{-2} \text{ h}^{-1}$ and -
413 $0.13 \pm 0.03 \text{ mg m}^{-2} \text{ h}^{-1}$, respectively.



414
415 **Figure 4.** Soil moisture (%) and soil temperature (°C) across three forest types: Ancient River
416 Terrace Forest (AR), White Sand Forest (WS), and Upland Forest (Up). Panels show (a) soil
417 moisture and (b) soil temperature. Different letters indicate statistically significant differences
418 between forest types ($p < 0.05$; $N = 36$), assessed using ANOVA for normally distributed data.

419 Boxes represent the median (horizontal line) and the interquartile range (IQR). Whiskers extend
420 to $1.5 \times$ IQR, and points represent individual observations

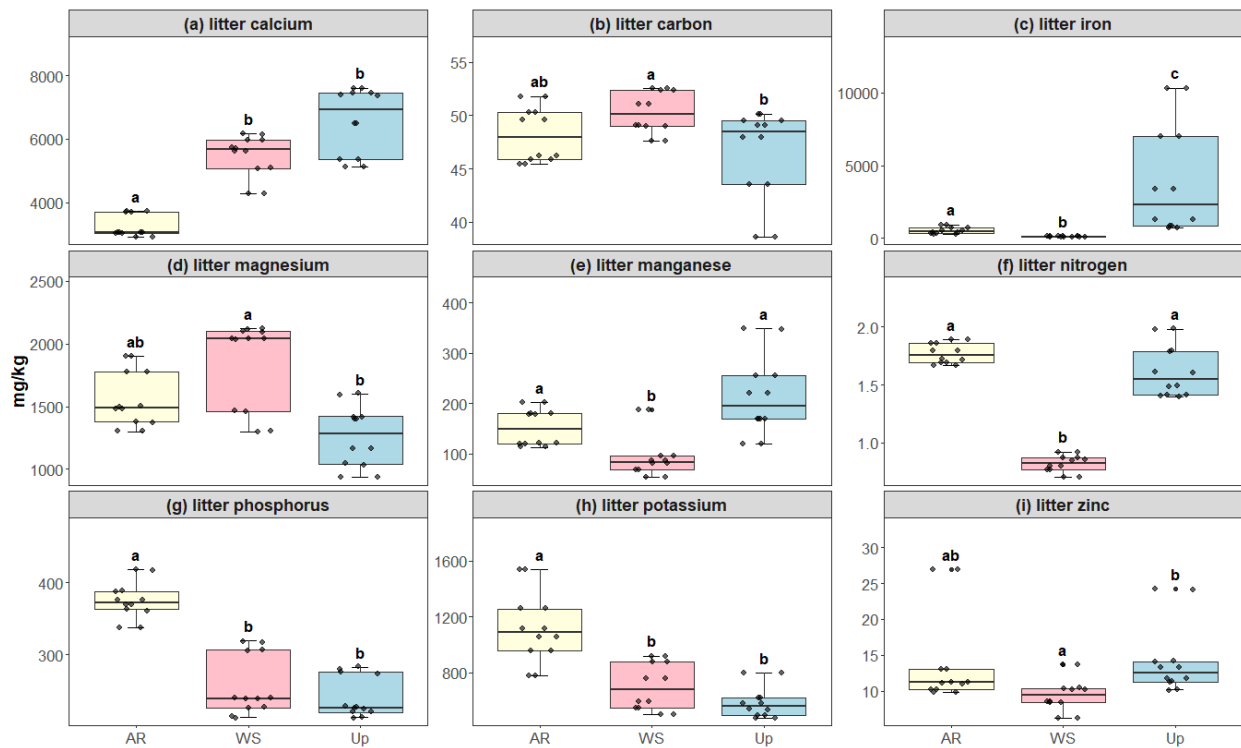
421 There were no statistically significant differences in soil moisture across forest types
422 (Fig. 4); however, the White Sand Forest showed the highest and the lowest soil moisture values.



423
424 **Figure 5.** Soil micro- and macronutrient concentrations across three forest types: Ancient River
425 Terrace Forest (AR), White Sand Forest (WS), and Upland Forest (Up). Panels show (a)
426 aluminum, (b) calcium, (c) carbon, (d) iron, (e) magnesium, (f) manganese, (g) nitrogen, (h) soil
427 pH, (i) phosphorus, (j) potassium, and (k) zinc. Different letters indicate statistically significant
428 differences between forest types ($p < 0.05$; $N = 36$). Differences were assessed using ANOVA
429 for normally distributed data (aluminum) and the Kruskal–Wallis test for non-normal data
430 (carbon, calcium, iron, potassium, magnesium, manganese, nitrogen, phosphorus, pH, and zinc).
431 Boxes represent the median (horizontal line) and the interquartile range (IQR). Whiskers extend
432 to $1.5 \times$ IQR, and points represent individual observations.

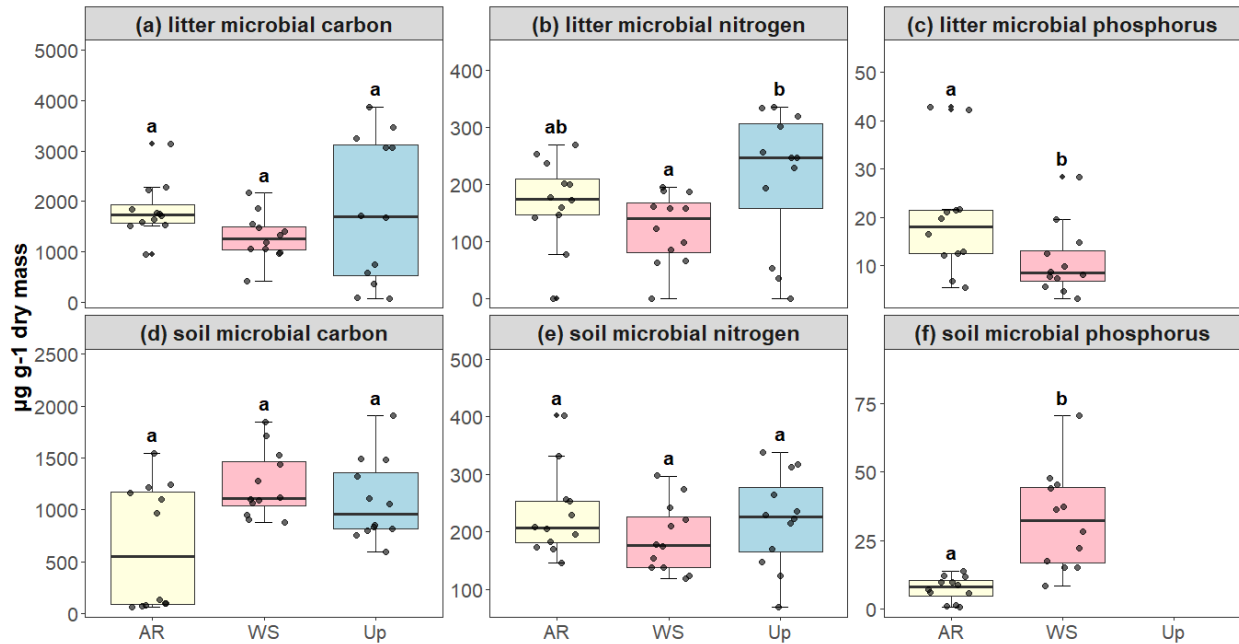
433 Soil macro- and micronutrients varied considerably between the forest types, with statistically
434 significant differences in carbon, magnesium, phosphorus, and iron for the White Sand Forest.

435 Phosphorus content was the highest in the White Sand Forest compared to other forest types
 436 (Fig. 5). All litter nutrients exhibited significant differences between forest types: Upland Forest
 437 showed the highest average concentrations of calcium, iron, manganese, and zinc, while the
 438 Ancient River Terrace Forest had the highest nitrogen, potassium, and phosphorus
 439 concentrations, and the White Sand Forest had slightly higher carbon concentrations (Fig. 6).



440

441 **Figure 6.** Litter micro- and macronutrient concentrations across three forest types: Ancient River
 442 Terrace Forest (AR), White Sand Forest (WS), and Upland Forest (Up). Panels show (a) calcium,
 443 (b) carbon, (c) iron, (d) magnesium, (e) manganese, (f) nitrogen, (g) phosphorus, (h) potassium,
 444 and (i) zinc. Different letters indicate statistically significant differences between forest types (p
 445 < 0.05 ; $N = 36$). Differences were assessed using ANOVA for normally distributed data
 446 (potassium and nitrogen) and the Kruskal–Wallis test for non-normal data (carbon, calcium, iron,
 447 magnesium, manganese, phosphorus, and zinc). Boxes represent the median (horizontal line) and
 448 the interquartile range (IQR). Whiskers extend to $1.5 \times$ IQR, and points represent individual
 449 observations.



450

451 **Figure 7.** Microbial biomass of carbon (C), nitrogen (N), and phosphorus (P) in litter and soil
 452 across three forest types: Ancient River Terrace Forest (AR), White Sand Forest (WS), and
 453 Upland Forest (Up). Panels show (a) litter microbial carbon, (b) litter microbial nitrogen, (c)
 454 litter microbial phosphorus, (d) soil microbial carbon, (e) soil microbial nitrogen, and (f) soil
 455 microbial phosphorus. Different letters indicate statistically significant differences between
 456 forest types ($p < 0.05$; $N = 36$). Differences were assessed using ANOVA for normally
 457 distributed data (litter microbial carbon, soil microbial nitrogen, and soil microbial phosphorus)
 458 and the Kruskal–Wallis test for non-normal data (soil microbial carbon, litter microbial nitrogen,
 459 and litter microbial phosphorus). Boxes represent the median (horizontal line) and the
 460 interquartile range (IQR). Whiskers extend to $1.5 \times$ IQR, and points represent individual
 461 observations.

462

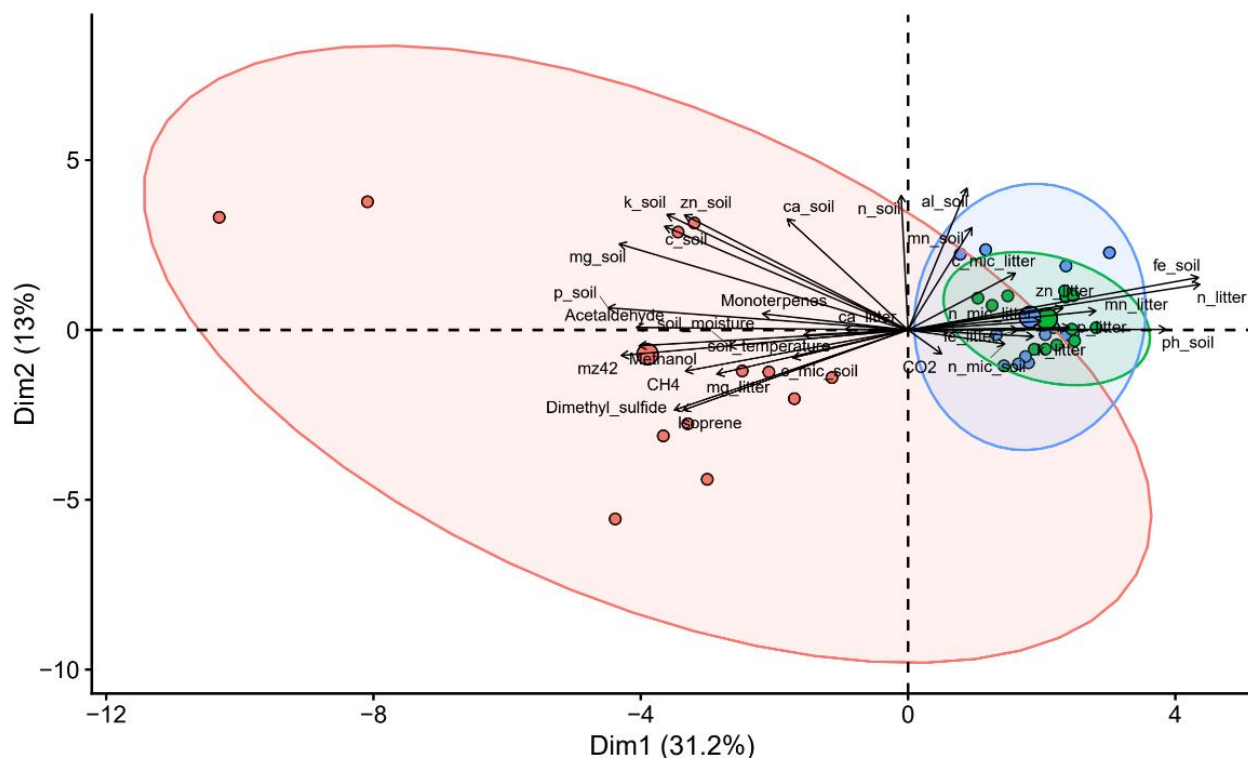
463 Microbial biomass (soil and litter), used here as a proxy for microbial activity, showed
 464 significant differences between forest types only for soil phosphorus, which was higher in the
 465 White Sand Forest compared to the Ancient River Terrace Forest (no data available for the
 466 Upland Forest). For carbon and nitrogen, significant differences were observed only in litter
 467 microbial biomass, with the upland forest exhibiting the highest values and the white sand forest

468 the lowest. However, for most microbial biomass parameters measured across soil and litter,
469 differences between forest types were not statistically significant (Fig. 7).

470 3.2 Identification of drivers of BVOC and GHG fluxes

471 3.2.1 Principal Component Analysis

472 A PCA of soil and litter characteristics and microbial biomass, and gas fluxes (BVOC
473 and GHG) indicated that PC1 and PC2 axes accounted for 48.5% of the data variation (Fig. 8).
474 The first axis explained 31.6% and the second 12.6% (Table 3). The PCA grouped forest types
475 into two distinct groups: Ancient River Terrace and Upland Forests showed considerable
476 overlap, with lower fluxes linked to litter characteristics, soil and litter microbial biomass, CO₂,
477 and soil pH. In contrast, the White Sand Forest formed a separate group with higher fluxes
478 associated with soil temperature, moisture, and elevated levels of phosphorus, magnesium, and
479 potassium.



480

481 **Figure 8.** PCA wherein the vectors reflect their correlation with the variables, and the colored
 482 circles represent the average PCA score related to each ambient. The analyzed variables are
 483 BVOCs (methanol, m/z 42, acetaldehyde, DMS, isoprene and monoterpenes), greenhouse gases
 484 (methane and CO₂), soil characteristics (carbon, nitrogen, phosphorus, potassium, calcium,
 485 magnesium, aluminum, iron, zinc, manganese, pH, temperature, and soil moisture), litter
 486 characteristics (carbon, nitrogen, calcium, magnesium, potassium, iron, zinc, manganese), and
 487 soil and litter microorganism dynamics (soil microbial nitrogen, soil microbial phosphorus, soil
 488 microbial carbon, litter microbial nitrogen, litter microbial phosphorus and litter microbial
 489 carbon). AR = Ancient River Terrace Forest, Up = Upland Forest, WS = White Sand Forest

490 **Table 3.** Percentage correlation values extracted from PCA; Fig. 8.

	PC1		PC2
Soil phosphorus	-85.95	Soil aluminum	79.94
Litter nitrogen	83.61	Soil nitrogen	75.89
Soil Iron	83.19	Soil potassium	65.06
Soil magnesium	-89.16	Soil zinc	64.85
m/z 42	-82.16	Soil calcium	62.61
Acetaldehyde	-77.85	Soil carbon	58.37
Methanol	-77.04	Soil manganese	57.77
Soil pH	73.93	Soil magnesium	48.50

491

492 3.2.2 Linear regression models for different forest types

493 We used linear regression models (referred to as linear models) to better understand the
 494 relationships between predictor variables and fluxes, as identified by the PCA analyses. Flux
 495 predictors showed substantial variation between the forest types (Fig. S3a, b, S4a, b, and S5a, b,
 496 in Section 5; supplementary material). Model comparisons for each forest type revealed
 497 similarities between Ancient River Terrace Forest and Upland Forests (Table 4). In contrast, the
 498 White Sand Forest was distinct (Table 4), as also shown by the PCA analysis.

499 In the Ancient River Terrace Forest, linear models for gas fluxes and predictor variables
 500 showed coefficients of determination (R²) above 0.8 for methanol, acetaldehyde, isoprene, and
 501 monoterpenes (Table 4). The most important nutrients for predicting gas fluxes from this forest
 502 type were potassium, manganese, magnesium, iron, carbon, and phosphorus. The linear models

503 for monoterpenes had soil microbial biomass carbon and litter potassium as predictors. The
 504 linear models for GHG had soil temperature, soil moisture, and litter nutrients as predictors.

505 **Table 4.** Multiple linear regression models with soil and litter characteristics and microbial
 506 biomass as predictors of gas fluxes in the three forest types – Ancient River Terrace Forest (AR),
 507 Upland Forest (Up), and White Sand Forest (WS). B = unstandardized coefficients. CI =
 508 confidence interval. f^2 = Cohen’s f^2 effect size. R^2 = R-squared value. R^2_{adj} = Adjusted R-squared
 509 value. N = 36.

510

Forest Type	Gas	R^2/R^2_{adj}	Predictor Variable	B	95% CI	P	f^2
AR	Methanol	0.83/0.80	Soil potassium	0.03	0.02; 0.04	< .001	1.92
			Litter nitrogen	0.02	0.01; 0.03	< .001	2.31
	Acetaldehyde	0.62/0.54	Soil iron	0.00	-0.00;0.00	0.05	0.12
			Soil manganese	0.004	0.00;0.00	0.00	1.58
	Dimethyl sulfide	0.57/0.47	Soil magnesium	0.006	0.00;0.00	0.2	0.05
			Litter magnesium	-0.004	-0.01;0.00	0.01	1.06
	Isoprene	0.96/0.95	Soil Phosphorus	0.00	0.00; 0.00	< .001	15.03
			Litter Phosphorus	0.06	0.04;0.07	< .001	9.38
	Monoterpenes	0.81/0.76	Soil microbial carbon	0.00	0.00; 0.00	0.08	4.26
			Soil Moisture	0.03	0.00; 0.05	< .001	0.05
Methane	0.27/0.20	Soil moisture	0.00	0.00; 0.00	0.08	0.5	
		Litter carbon	0.00	0.00;0.00	0.02	0.32	
CO ₂	0.68/0.61	Soil temperature	9.05	3.10; 15.0	0.00	1.23	
		Litter phosphorus	-87.94	-156; -19	0.01	0.94	
Up	Methanol	0.61/0.53	Soil potassium	0.61	0.18; 1.0	0.01	0.17
			Soil microbial nitrogen	0.00	0.00; 0.00	0.00	1.44
	m/z 42	0.68/0.60	Soil potassium	0.00	0.00; 0.00	0.00	0.73
			Soil microbial	0.00	0.00; 0.00	0.00	1.50

		nitrogen					
Acetaldehyde	0.60/0.52	Soil iron	0.00	0.00; 0.00	0.14	0.17	
		Litter microbial carbon	0.02	0.00; 0.00	0.00	1.38	
Dimethyl sulfide	0.74/0.69	Litter microbial carbon	0.00	0.00; 0.00	<0.001	1.10	
		Litter microbial nitrogen	0.00	0.00; 0.00	0.003	1.85	
Isoprene	0.77/0.72	Soil carbon	0.00	0.00; 0.00	0.007	1.25e-03	
		Liter magnesium	0.00	0.00; 0.00	< .001	5.94	
Monoterpenes	0.79/0.74	Soil potassium	1.6	0.94;2.3	< .001	0.96	
		Litter microbial nitrogen	0.00	0.00;0.00	< .001	2.86	
Methane	0.88/0.86	Soil carbon	0.231	0.00; 0.00	0.043	0.06	
		Soil moisture	0.00	0.00; 0.00	< .001	7.91	
CO ₂	0.62/0.54	Litter microbial nitrogen	0.00	0.01; 0.06	0.025	0.25	
		Litter microbial carbon	0.00	0.00;0.00	0.00	1.43	
Methanol	0.82/0.79	Soil temperature	-3.0	-4.4, -1.5	< 0.001	2.60	
		Litter phosphorus	-8.4	-16, -0.37	< 0.042	0.62	
m/z 42	0.86/0.83	Soil moisture	0.187	0.09; 0.27	< .001	2.93	
		Litter nitrogen	-54.19	-75.90; -32.49	< .001	3.54	
Acetaldehyde	0.65/0.57	Soil moisture	1.368	0.28; 2.45	0.019	1.02	
		Litter nitrogen	-327.4	-593; -61	0.021	0.86	
Dimethyl sulfide	0.76/0.71	Soil temperature	-0.06	-0.09; -0.03	0.00	1.87	

WS

		Soil phosphorus	-0.06	-0.09, -0.03	0.003	1.36
Isoprene	0.76/0.71	Soil temperature	-2.3	-3.6; -0.96	0.004	1.70
		Soil phosphorus	-0.05	-0.07; -0.02	0.003	1.54
Monoterpene	0.85/0.82	Soil moisture	0.13	0.06; 0.20	0.003	0.36
		Litter nitrogen	2.1	1.5; 2.8	< 0.001	5.66
Methane	0.50/0.39	Soil moisture	0.00	0.0; 0.0	0.027	0.35
		Litter zinc	0.00	0.0; 0.0	0.035	0.69
CO ₂	0.74/0.68	Soil microbial carbon	0.02	0.0; 0.03	0.029	1.07
		Litter zinc	3.5	1.6; 5.5	0.003	1.81

511

512 For the Upland Forest, linear models for gas fluxes showed R² higher than 0.8 for
513 isoprene and methane (Table 4), and key nutrients for predicting gas fluxes included potassium,
514 iron, manganese, and carbon. Microbial biomass was significant in predicting gases like
515 methanol and DMS. Acetaldehyde and isoprene shared soil iron and manganese as predictors,
516 while DMS and CO₂ were linked to litter carbon and microbial nitrogen.

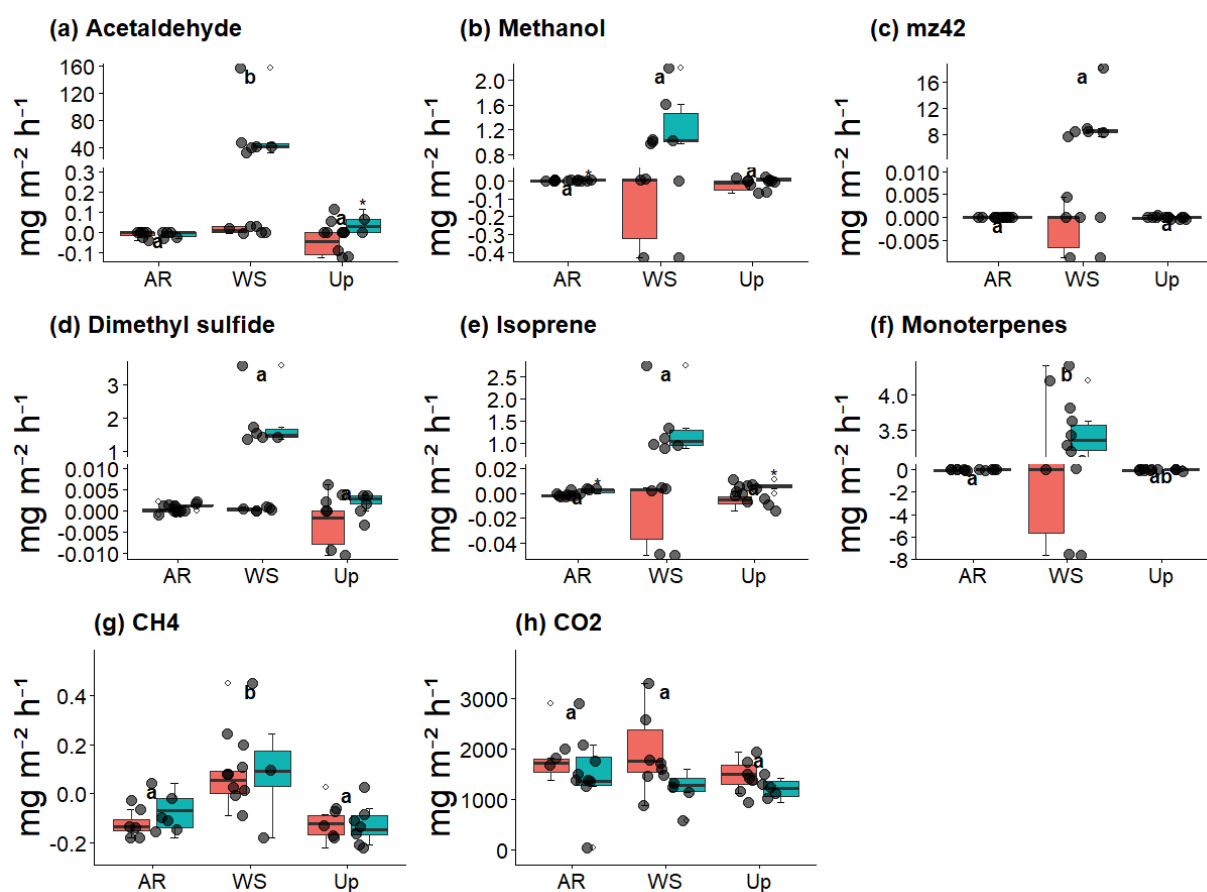
517 In the White Sand Forest, linear models showed R² higher than 0.8 for methanol, m/z 42,
518 and monoterpenes (Table 4). Key nutrient predictors included phosphorus, nitrogen, and zinc.
519 All emitted gases (except CO₂) were influenced by soil temperature or moisture. Soil
520 temperature was inversely related to fluxes of methanol, DMS, and isoprene, while emissions of
521 m/z 42, acetaldehyde, monoterpenes, and methane increased with soil moisture.

522

523 3.3 Spatial variability within forest types

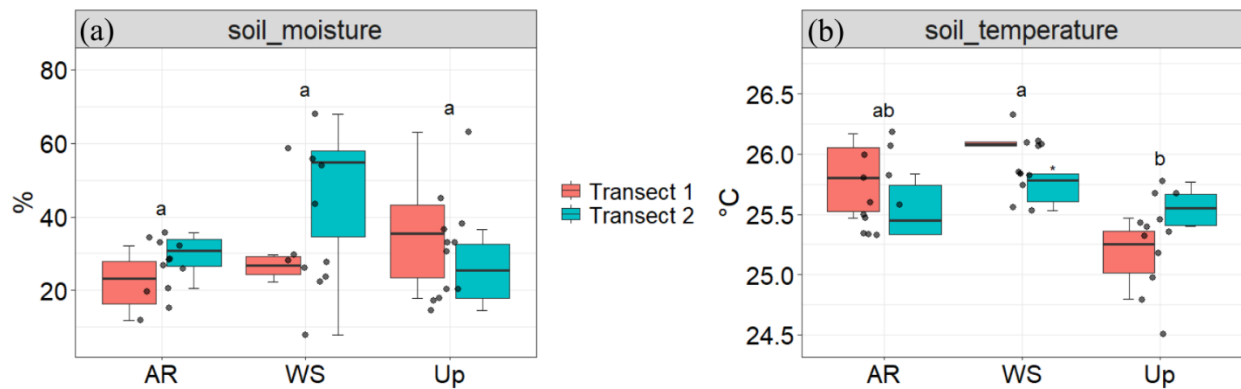
524 Figure 9 shows BVOC and GHG fluxes of each Transect, Figure 10 shows soil
525 temperature and soil moisture of each Transect, and Figure 11 illustrates the spatial variability
526 within and between Transects for isoprene and monoterpenes (see supplementary material,

527 Section 8; Fig. S8, S9, and S10 for other gases). In the Ancient River Terrace Forest, BVOC
 528 fluxes were generally lower in Transect 1, while GHG fluxes were similar between Transects
 529 (Fig. 9); soil temperature was higher in Transect 1, while Transect 2 was slightly wetter
 530 (although not statistically significant) (Fig.10). White Sand Forest exhibited the greatest
 531 variation between Transects, with the highest BVOC emissions in Transect 2, and significant
 532 variations in acetaldehyde, m/z 42, DMS, isoprene, and methanol; monoterpene fluxes showed
 533 high variation in emissions and consumption in Transect 1, while Transect 2 had low variation
 534 and high emissions; and methanol was emitted in Transect 1 and consumed in Transect 2. In the
 535 Upland Forest, significant differences between Transects were noted for acetaldehyde, m/z 42,
 536 DMS, and isoprene.



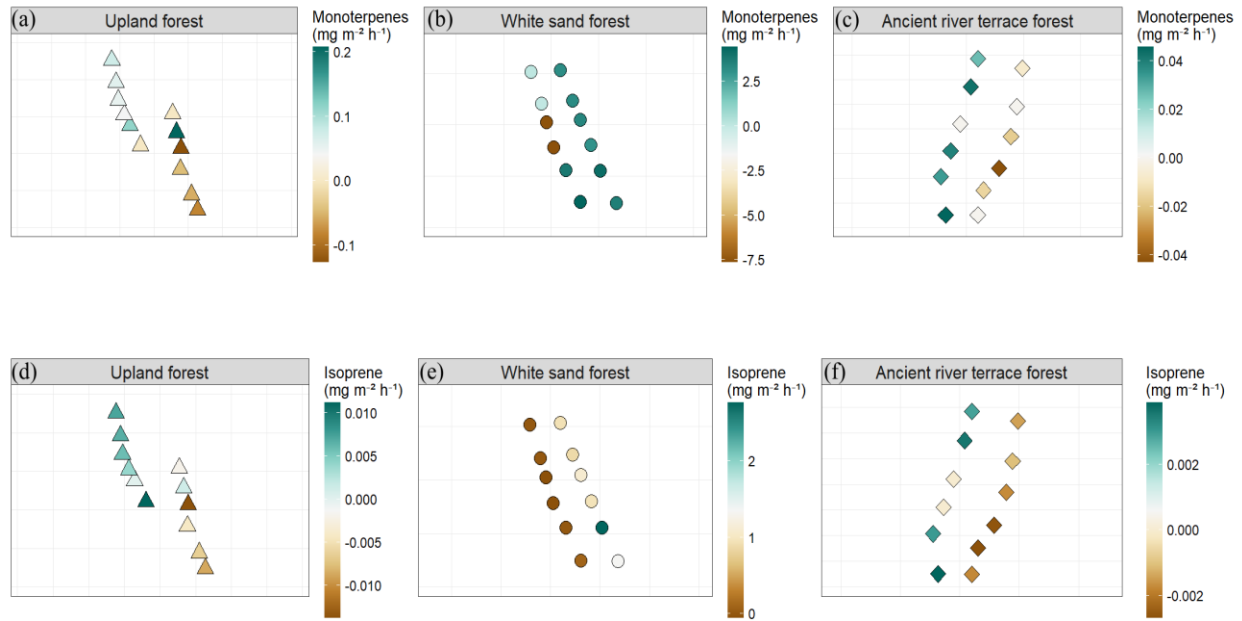
537
 538 **Figure 9.** Soil-litter BVOC and greenhouse gas (GHG) fluxes across three forest types and their
 539 respective transects: Ancient River Terrace Forest (AR), White Sand Forest (WS), and Upland
 540 Forest (Up). Panels show (a) acetaldehyde, (b) methanol, (c) m/z 42, (d) dimethyl sulfide (DMS),

541 (e) isoprene, (f) monoterpenes, (g) methane (CH₄), and (h) carbon dioxide (CO₂). Colors indicate
 542 the two transects within each forest type. Different letters indicate statistically significant
 543 differences between forest types ($p < 0.05$; $N = 36$), assessed using the Kruskal–Wallis test for
 544 non-normal data. Boxes represent the median (horizontal line) and the interquartile range (IQR).
 545 Whiskers extend to $1.5 \times$ IQR, and points represent individual observations. For panels (a–f), the
 546 y-axis is broken and displayed on two scales to improve the visualization of variation in flux
 547 values.



548

549 **Figure 10.** Soil moisture (%) and soil temperature (°C) across three forest types and their
 550 respective transects: Ancient River Terrace Forest (AR), White Sand Forest (WS), and Upland
 551 Forest (Up). Panels show (a) soil moisture and (b) soil temperature. Colors indicate the two
 552 transects within each forest type. Different letters indicate statistically significant differences
 553 between forest types ($p < 0.05$; $N = 36$), assessed using ANOVA for normally distributed data.
 554 Boxes represent the median (horizontal line) and the interquartile range (IQR). Whiskers extend
 555 to $1.5 \times$ IQR, and points represent individual observations.



556

557 **Figure 11.** Spatial distribution of BVOC fluxes across sampling points within the three forest
 558 types: Upland Forest, White Sand Forest, and Ancient River Terrace Forest. Panels show
 559 monoterpene fluxes (a–c) and isoprene fluxes (d–f), expressed in $\text{mg m}^{-2} \text{h}^{-1}$. Each forest type
 560 includes two transects sampled on consecutive days, with six sampling points per transect ($N =$
 561 12 per forest type). Points represent individual chamber locations along each transect, illustrating
 562 the spatial heterogeneity of BVOC emissions within the forest plots.

563

564 4. Discussion

565 Previous studies investigating tropical soil BVOC fluxes using in-situ measurements and
 566 incubation (Bourtsoukidis et al., 2018) and fertilization experiments (Llusià et al., 2022) showed
 567 that fluxes were higher than previously anticipated. Although these pioneer studies were very
 568 important to understand soil BVOC fluxes from the tropics, our study took one step further by
 569 investigating soil-litter BVOC and GHG fluxes across Amazonian Forest types. We found that
 570 soil-litter BVOC and GHG fluxes changed across forest types and were influenced by
 571 differences in nutrient content, soil moisture, temperature, and microbial biomass. Given the
 572 extensive number of measured variables, we chose to focus our discussion on the key
 573 observations related to BVOC and methane fluxes and their drivers, rather than covering all
 574 variables and fluxes. However, since these variables may still be of interest to the reader, detailed

575 analyses are provided in the supplementary material (Section 2). In the following sections, we
576 first compare soil–litter properties among forest types, followed by a comparison of observed
577 BVOC and GHG fluxes both between forest types and with other tropical studies. We then
578 discuss their potential drivers and the broader significance of our findings.
579

580 **4.1 Differences in soil and litter nutrient contents across forest types**

581 Variations in soil and litter properties were observed among forest types, particularly
582 concerning their total nutrient contents. These total nutrient pools reflect long-term nutrient
583 availability and reservoirs within each ecosystem, shaped by distinct biogeochemical processes.
584 In the Ancient River Terrace Forest, high concentrations of potassium and phosphorus were
585 found in the litter, suggesting strong nutrient retention and efficient cycling within this forest
586 type. This may result from its history of periodic flooding and the presence of allisols—relatively
587 young, nutrient-rich soils (Andreae et al., 2015).

588 In the Upland Forest, the dominance of soil iron total content is likely related to the
589 intense leaching common in its ferrasols (oxisols), resulting in iron enrichment due to the
590 removal of other nutrients (Mosquera et al., 2024). In addition, the formation of iron oxides can
591 reduce the mineralization of organic matter, promoting iron accumulation in the leaf litter (Li et
592 al., 2023). The White Sand Forest showed differences in soil properties when compared to the
593 other forest types analyzed. Despite its well-documented low fertility (Mendonça et al., 2015;
594 Demarchi et al., 2022) and arenosol characteristics, this forest type displayed unexpectedly high
595 soil phosphorus and carbon total concentrations. Phosphorus total concentrations, for instance,
596 were up to four times higher than in Upland and Ancient River Terrace Forests. This observation
597 may possibly reflect the role of dissolved organic nutrients in mitigating nutrient limitations
598 (Lange et al., 2024), or the efficient capture and retention of nutrients within the forest’s
599 extensive root mats, which can enhance carbon storage and nutrient cycling in structurally
600 analogous ecosystems (Draper et al., 2014). Furthermore, iron total concentrations in the soil of
601 this forest were lower than expected (Cornu et al., 1997), possibly attributed to spatial variability
602 and seasonal dynamics. During the dry season, the low water-retention capacity of sandy soils
603 leads to drought stress, whereas in the wet season, leaching redistributes iron, aluminum, and

604 magnesium (García-Villacorta et al., 2016) – a process that can form cemented horizons,
605 impeding drainage and elevating water tables (Franco & Dezzeo, 1994; Demarchi et al., 2022).
606 Variable iron concentrations, together with wet-season leaching and elemental redistribution,
607 shape the White Sand Forest into a highly distinct environment. In addition, tree species
608 composition could play a role in influencing nutrient stocks in this forest type (García-Villacorta
609 et al., 2016; Gomes Alves et al., 2022).

610

611 **4.2 Differences in Gas Fluxes across Forest Types**

612 Here, by comparing forest type fluxes, it is important to recognize that our chamber
613 measurements represent the combined (net) flux from both soil and litter. Observed differences
614 between sites may therefore reflect variations in the relative contributions of soil and litter, for
615 example, due to different amounts of litter. The amount of litter in the chambers was not
616 quantified, although we generally observed more litter in the White Sand Forest and Ancient
617 River Terrace Forest. These patterns may also vary seasonally as litter inputs and decomposition
618 rates change throughout the year (Rodrigues et al., 2023), potentially contributing to local
619 differences in soil–litter gas fluxes. Because our measurements do not allow us to separate these
620 sources, we treat soil and litter as a single compartment in our analysis and discuss differences in
621 combined soil–litter fluxes across forest types. Future studies should include measurements of
622 litter mass and species composition to better constrain their influence on gas exchange.

623 The White Sand Forest exhibited the highest emissions and consumption of BVOCs and
624 GHGs, accompanied by the greatest chemical diversity in gas fluxes. Plant species endemic to
625 this ecosystem may influence BVOC emission patterns and their chemical speciation: Fine et al.
626 (2004, 2006) showed that tree species adapted to very nutrient-poor sandy soils highly invest in
627 secondary metabolite compounds in defense against herbivory, since leaves are very
628 energetically costly for the plant. This large quantity of secondary compounds can directly
629 influence litter decomposition rate (Chomel et al., 2016) and probably release gases and various
630 compounds into the soil and water (Caetano, 2022).

631 No clear differences between forest types were observed for the soil–litter CO₂ exchange
632 fluxes. The large variation at the local scale, both within and between forest types, has previously
633 been reported for a central Amazonian field site (van Asperen et al., 2020). Overall, the values
634 measured in this study fall within the range commonly reported for soil respiration in Amazonian
635 forests. Previous studies across different forest types in central Amazonia have documented soil
636 CO₂ fluxes typically between ~2 and 6 μmol m⁻² s⁻¹ (corresponding roughly to 320–950 mg m⁻²
637 h⁻¹), with fluxes largely depending on soil moisture and temperature conditions (van Asperen et
638 al., 2020; Chambers et al., 2004; Doff Sotta et al., 2004).

639 Isoprenoids were emitted in considerable amounts in the White Sand Forest. As
640 isoprenoids are not expected to be emitted from soil (Bach & Rohmer, 2013; Asensio et al.,
641 2008), the observed high emissions might indicate contributions from the activity of
642 microorganisms living in the soil and litter (Carruthers & Lee, 2021; Hernandez-Arranz et al.,
643 2019). In addition, it is important to note that, although emissions in this study are expected to
644 come from soil and litter, the contribution of root emissions cannot be ruled out, as the main
645 source of isoprenoids is expected to be plant metabolism (Pulido et al., 2012; Thulasiram et al.,
646 2007).

647 A previous study on experimental rainforest soils - similar to Upland Forest soils -
648 showed BVOC soil uptake (under wet conditions) primarily for isoprenoids, carbonyls, and
649 alcohols, as well as soil emissions of DMS and carbonyl compounds such as acetaldehyde and
650 acetone (Pugliese et al., 2023). Our Upland Forest isoprene fluxes exhibited lower soil uptake (-
651 0.005 mg m⁻² h⁻¹) compared to the increased uptake fluxes under drier conditions (~ -2.38 mg
652 m⁻² h⁻¹) observed by Pugliese et al. (2023). This lower isoprene uptake by the soil observed in
653 the Upland Forest likely reflects microbial assimilation and/or abiotic sorption processes acting
654 on atmospheric isoprene within the soil–litter compartment. These processes are strongly
655 influenced by forest structural attributes and underlying soil properties, which are likely different
656 between this study and Pugliese et al. (2023). Additionally, the higher atmospheric isoprene
657 concentrations reported by Pugliese et al. (2023) compared with those in this study may help
658 explain the greater soil isoprene uptake observed in their work.

659 In general, our Upland and Ancient River Terrace Forests showed lower average
660 emissions and uptake than those reported by Pugliese et al. (2023). A study focusing on
661 methanol fluxes in cropland soils observed values ranging from 0.53 to 2.93 mg m⁻² h⁻¹ (Liu et
662 al., 2024), which are higher than those observed in our study in Upland and Ancient River
663 Terrace Forests but comparable to the White Sand Forest fluxes (0.61 ± 0.81 mg m⁻² h⁻¹). These
664 higher emissions in crop soils can likely be attributed to factors such as crop species, tillage,
665 fertilization, and irrigation, which can all influence BVOC emission rates; whereas the high
666 methanol emission observed in our study could be related to the root growth of White Sand
667 Forest's extensive root mats, although future studies are necessary to confirm this hypothesis.

668 The highest DMS emissions were observed in the White Sand Forest (~ 1.10 ± 1.14 mg
669 m⁻² h⁻¹), which were higher than the DMS emission of 5.76 µg m⁻² h⁻¹ reported by Jardine et al.
670 (2015) for Amazon soils. However, while an interesting observation, it is important to note that
671 the high magnitude of DMS fluxes presented here might partly be caused by a potential
672 agglomerate of acetaldehyde (mass 45) with water, resulting in the same mass as DMS (63),
673 suggesting that future studies should make use of techniques that differentiate these compounds.

674 A compound with a mass-to-charge ratio (m/z) of 42 was observed in the White Sand
675 Forest, but its identity could not be confirmed due to technical limitations (Dunne et al., 2012).
676 This m/z 42 is frequently attributed to acetonitrile, a known biomass burning marker primarily
677 associated with anthropogenic sources (Huangfu et al., 2021). However, since it can also be
678 emitted by microorganisms (Raio et al., 2020), it is possible that the microbial communities of
679 the White Sand Forest contributed to potential acetonitrile (m/z 42) emissions.

680 Methane uptake was observed in the Upland (-0.12 mg m⁻² h⁻¹) and Ancient River
681 Terrace Forests (-0.10 mg m⁻² h⁻¹), whereas emissions were observed in the White Sand Forest
682 (0.12 mg m⁻² h⁻¹). In another central Amazonia site, Upland Forest methane fluxes of similar
683 magnitude were observed (-0.02 to -0.09 mg m⁻² h⁻¹) (van Asperen et al., 2020). However, the
684 discrepancy in White Sand Forest fluxes, with uptake reported in their study (-0.38 to -0.25 mg
685 m⁻² h⁻¹) and emissions observed here, can likely be attributed to the high spatial variability
686 characteristic of white sand forest ecosystems.

687

688 4.3 Drivers of Soil and Litter Gas Fluxes

689 4.3.1 Soil moisture and soil temperature as drivers of soil-litter gas fluxes

690 A PCA was initially conducted to identify variables that might differentiate forest types
691 and their gas fluxes. However, due to the overlapping ellipses and limited discrimination
692 capacity, linear models were applied to further explore the findings. These models highlighted
693 soil temperature and moisture as key physical drivers across all three forest types, aligning with
694 observations in other ecosystems (Trowbridge et al., 2020; Pugliese et al., 2023; Liu et al., 2024).

695 Nevertheless, before evaluating these key drivers, it is important to recognize that
696 external factors inevitably influence soil moisture and temperature. Although transects were
697 consistently measured at the same time (08:00–10:00 local time), they were conducted on
698 consecutive days under varying weather conditions. In addition, while radiation was not
699 quantified during the campaign, its effects should be considered. Despite the use of opaque
700 chambers, the chamber surrounding environment - and thus the prevailing BVOC flux dynamics
701 - may still be modulated by incoming radiation. These factors are particularly important in the
702 White Sand Forest, where the open canopy, short stature, and shallow water table (Adeney et al.,
703 2016; Rossetti et al., 2019) promote highly dynamic conditions, reflected in the strong variability
704 of soil temperature and moisture between consecutive transects. While on one hand these factors
705 represent a limitation, it also allowed us to explore the influence of external factors on gas fluxes
706 within the same forest type, such as the rain event, which will be discussed hereafter.

707 In addition to the complicating external factors, we should also note that high soil
708 moisture values were generally accompanied by lower soil temperatures, thereby complicating
709 separating individual drivers. A similar pattern was observed by van Asperen et al. (2024), who
710 showed that the direct effects of temperature and moisture are difficult to differentiate under
711 tropical field conditions, where temperature variation is usually small. Furthermore, it should be
712 noted that this study is additionally limited by a small temporal dataset. Thus, although some
713 BVOC fluxes showed a positive association with soil moisture and a negative association with
714 soil temperature, distinguishing the primary driver remains difficult. Nevertheless, despite the
715 limitations described above, we discuss the expected effects of soil moisture and temperature on
716 our fluxes below.

717 We observed a negative relationship between temperature and certain BVOC fluxes, but
718 we interpret this as an indirect effect mediated by the previously described link to soil moisture.
719 In general, elevated temperatures are expected to enhance both BVOC emissions and biological
720 uptake, as described by Baggesen et al. (2022). If the temperature sensitivity of uptake exceeds
721 that of emission, this may result in reduced net emissions or even a net sink for BVOCs (Asensio
722 et al., 2007; Peñuelas et al., 2014; Jiao et al., 2023).

723 For soil moisture, we found a clear relation with most of the BVOC fluxes, especially for
724 the White Sand Forest. The effects of moisture on BVOC fluxes were also described by Pugliese
725 et al. (2023), who reported that rainforest soils acted as net BVOC sinks under moist conditions
726 and as net BVOC sources under dry conditions. In the Upland Forest, we observed a similar
727 pattern as Pugliese et al (2023), with the wetter Transect showing BVOC consumption while the
728 drier Transect showed emissions. The White Sand Forest showed even stronger inter-Transect
729 differences, with high BVOC emissions observed in the wetter Transect, and low emissions and
730 uptake observed in the drier Transect. The pronounced differences between these Transects
731 suggest that the rainfall event preceding Transect 2 was an important driver of the observed
732 variation. A similar hypothesis was posed by Bourtsoukidis et al. (2018), who also observed that
733 sesquiterpene emissions from Upland Forest soils in the dry season (after a rain event) were
734 comparable to those from vegetation. In addition to increasing soil moisture, the physical impact
735 of rainfall may trigger short-term emission bursts (Miyama et al., 2020). As we observed
736 substantially high isoprene, monoterpenes, and acetaldehyde emissions in Transect 2 of the
737 White Sand Forest, we argue that these observed BVOC emissions represent a burst induced by
738 the preceding rainfall event. Similar observations have been reported by Greenberg et al. (2012),
739 who observed increased BVOC emissions during and immediately after rainfall in a Ponderosa
740 pine plantation, and by Jardine et al. (2015), who reported a peak in soil DMS emissions
741 following rainfall.

742 Overall, we hypothesize that the rainfall event induced an emission burst, mostly
743 explaining the elevated BVOC fluxes observed in that transect. Nevertheless, interactions
744 between soil temperature, soil moisture, and BVOC fluxes remain highly complex across
745 heterogeneous forest types, with external drivers contributing to strong spatial and temporal
746 variability and making their combined effects difficult to separate under natural field conditions.

747

748 **4.3.2 Forest Type-specific Drivers of Soil-litter Gas Fluxes**

749 We observed that drivers of soil and litter gas fluxes varied across forest types, reflecting
750 their unique environmental conditions and nutrient dynamics. In general, Ancient River Terrace
751 and Upland Forests showed many similarities in the predictors of certain gases, while other
752 drivers were found for the White Sand Forest. Here, we focus on the key factors influencing gas
753 fluxes: soil nutrients, microbial biomass, and their interactions with environmental conditions.

754 Soil potassium was found to be a significant factor influencing Ancient River Terrace
755 and Upland Forest fluxes, being identified as a predictor of methanol and monoterpenes. In
756 addition, it was also identified as a predictor of m/z 42 fluxes in the Upland Forest. Although we
757 did not find studies directly related to BVOCs and GHGs fluxes to soil potassium content,
758 potassium is an essential macronutrient for plant growth and metabolism. Its availability is
759 known to affect plant physiological processes (Wang et al., 2013), and its cycling within the soil
760 environment, often mediated by microbial activity, influences potassium's uptake by plants
761 (Mazahar & Umar, 2022). These plant- and soil-mediated processes can, in turn, indirectly
762 influence the BVOC production and release observed within the soil-litter compartment of our
763 study, by affecting the overall ecosystem health and the quality of organic matter available for
764 decomposition.

765 In the Upland Forest, our methane consumption fluxes correlated well with soil carbon
766 (in conjunction with soil moisture, as mentioned previously). Soil organic carbon is known to
767 play an important role in supporting methanotrophic bacteria, which are responsible for methane
768 oxidation (Lee et al., 2023); therefore, we suggest that the total soil carbon observed in our study
769 might affect methane uptake through a similar process. Phosphorus, like carbon, is a key nutrient
770 in the soil and significantly affects BVOC soil-litter fluxes, especially for methanol in the White
771 Sand Forest. The relationship between phosphorus and BVOC emissions is well documented for
772 plants since the availability of phosphorus can influence the production and emission of BVOCs
773 (Ndah et al., 2022). However, some fertilization studies have also shown that increasing soil
774 nutrient status (nitrogen, phosphorus, and potassium) can modify pH levels, affecting
775 microorganisms and their health state (Stotzky et al., 1976), which directly or indirectly

776 promotes or inhibits soil BVOC fluxes (Liu et al., 2024; Raza et al., 2017). Our findings with bi-
777 directional soil-litter fluxes in the White Sand Forest are consistent with these previous studies
778 showing an increase or inhibition of soil BVOC fluxes with soil nutrient content.

779 Interestingly, our results suggested that lower phosphorus levels were associated with
780 higher isoprene emissions. The mechanisms behind this relationship remain unclear. However,
781 studies on soil fertilization in tropical forests by Llusia et al. (2022) found that phosphorus
782 fertilization is less efficient than nitrogen fertilization in increasing monoterpene and
783 sesquiterpene emissions (they did not find isoprene emissions). They observed that emissions
784 increased when the soil was fertilized only with nitrogen - consistent with a phosphorus-limited
785 system - because excess nitrogen stimulates the enzymes responsible for producing
786 monoterpenes and sesquiterpenes. Conversely, the addition of phosphorus likely redirected this
787 nutrient toward plant growth, resulting in lower emissions of monoterpenes and sesquiterpenes in
788 the phosphorus-fertilized plots compared to those fertilized with nitrogen. As in this study, there
789 was no fertilization or a controlled environment, so we cannot draw similar conclusions.
790 However, our findings provide valuable insights into the possible interactions between
791 phosphorus, nitrogen, and soil-litter BVOC fluxes in tropical ecosystems. These observations
792 align with previous studies on the influence of soil nutrients (Liu et al., 2024; Llusia et al., 2022),
793 and we suggest future soil fertilization studies to explore these relationships across soil and forest
794 types in Amazonia.

795 For the Upland Forest, it was found that microbial biomass was a significant driver for
796 almost all soil-litter fluxes, except for isoprene and methane. This aligns with previous studies
797 that have identified microbial biomass as an important driver for soil-litter gas fluxes (Leff &
798 Fierer, 2008; Mancuso et al., 2015; Tang et al., 2019). For example, research on soil organic
799 matter degradation by Lehnert et al. (2024) demonstrated that it is an important source of DMS
800 emissions, highlighting the role of microorganisms associated with decomposition. Similarly,
801 studies on tropical plant litter VOC fluxes have shown that microbial processes within the litter
802 layer can strongly influence the production and consumption of volatile compounds (Crocker et
803 al., 2025). Jardine et al. (2015) point out that DMS emissions in Amazonian soil are related to
804 microbial processes, a relationship also reported in litter studies by Kesselmeier and Hubert
805 (2002). DMS can be produced in anaerobic environments, such as saturated soil or lakes

806 (Lehnert et al., 2024). This may explain the high emissions observed in transect 2 (wetter and
807 more saturated) of the White Sand Forest, where conditions favorable to anaerobic processes are
808 common and frequently linked to the production of sulfur compounds such as DMS. In contrast,
809 in the drier transect 1 of the upland forest, DMS consumption was observed, suggesting the
810 occurrence of microbial uptake processes. In fact, another study has shown that bacteria can
811 consume carbon from DMS as an energy source in soil and lake sediments (Eyice et al., 2015).
812 Therefore, the observed uptake may be the result of microorganisms utilizing the carbon present
813 in DMS as an energy source, leading to uptake rather than production. This dual role of
814 microorganisms - as both producers and consumers of DMS - highlights the complexity of sulfur
815 cycling in terrestrial ecosystems.

816 Based on the limited number of studies investigating the relationship between
817 microorganisms and BVOC dynamics, it has been shown that some Proteobacteria,
818 Actinobacteria, and Firmicutes can produce isoprene (Kuzma et al., 1995; McGenity et al.,
819 2018). *Bacillus subtilis* can produce isoprene in response to stress; however, the mechanism is
820 still not clear (McGenity et al., 2018). Some studies have shown that reduced microbial diversity,
821 whether in soil (Abis et al., 2020; Sillo et al., 2024) or associated with plant surfaces (Saunier et
822 al., 2020), can increase BVOC fluxes and alter the chemical composition of emitted compounds.
823 Although microbial community data were unavailable in this study, we suggest that potential
824 differences in microbial diversity may have influenced emission and consumption patterns.
825 Recent advances combining genomic, metabolomic, and isotopic approaches have begun to
826 directly link microbial metabolism with VOC production and transformation in soils (Hernandez
827 et al., 2023). Integrating such approaches with gas flux measurements would help to better
828 identify the microbial taxa and metabolic pathways involved in BVOC exchange. Therefore,
829 future studies should combine flux measurements with microbial community and functional
830 analyses to better understand these dynamics.

831

832 **4.4 The relevance of White Sand Forest ecosystems**

833 This study showed large variability across forest types and unexpectedly high BVOC
834 emissions from the White Sand Forest. In general, relatively few studies have been performed on

835 White Sand Forests, which is partly explained by the challenging conditions of this type of
836 forest, such as flooding and extreme temperatures (Adeney et al., 2016). In addition, the
837 scattered patches of differentiated vegetation distributed within extensive Upland Forests
838 (Demarchi et al., 2022) can make access to these sites even more difficult and require specific
839 infrastructure for data collection. While our observations constitute one of the first
840 characterizations of BVOCs in this unique forest type, their capacity to capture the full spectrum
841 of extreme conditions is inevitably limited by the short temporal coverage of the dataset. To the
842 best of our knowledge, only one study has provided data on BVOC fluxes with soil incubation
843 lab measurements (Bourtsoukidis et al., 2018), and another measuring GHGs in-situ (van
844 Asperen et al., 2020) in White Sand Forests. Despite representing only 5% of the Amazon basin
845 area (Adeney et al., 2016) and 8% of the Reserve of this study (Demarchi et al., 2022), White
846 Sand Forests are extremely important environments. Their sandy, nutrient-poor soil type has
847 created a challenging ecosystem for plant growth (Fine & Baraloto, 2016), and this unique
848 condition has selected specialized flora and fauna adapted to thrive in these ecosystems (Adeney
849 et al., 2016; Demarchi et al., 2022). This high level of endemism contributes significantly to the
850 overall biodiversity of the Amazon Basin (García-Villacorta et al. 2016). Moreover, White Sand
851 Forests have been shown to play a crucial role in the chemistry of dissolved organic matter
852 (DOM) in Amazonian blackwater rivers, linking terrestrial ecosystem processes to aquatic
853 biogeochemistry (Simon et al., 2021). Our results suggest a stronger link between White Sand
854 Forest gas fluxes and physical factors (more than other forest types), which indicates a possible
855 sensitivity to upcoming climate extremes. Although Costa et al. (2023) did not focus specifically
856 on the White Sand Forest, they showed that regions of the Amazon with shallow water tables -
857 such as the White Sand Forests - can act as hydrological refuges during droughts. In these areas,
858 higher productivity under dry conditions may maintain relatively stable carbon dynamics,
859 presenting a contrasting response to the substantial carbon losses typically observed in deep
860 water table, Upland Forests, during drought. In addition, a recent study reported high
861 atmospheric isoprene concentrations in the northwestern Amazon throughout most of the year
862 (Wells et al., 2022) - a region characterized by extensive and continuous White Sand Forest
863 cover (Borges et al., 2014). In this context, as White Sand Forests play a critical role in
864 regulating the carbon cycle and maintaining Amazonian biodiversity (Rossetti et al., 2019), our
865 study suggests that White Sand Forests may represent a significant source and sink of BVOCs.

866 Together, this highlights the need to better integrate White Sand Forests into future BVOC and
867 GHG flux studies and Earth System modeling.

868

869 **5. Summary and future directions**

870 Multiple interconnected factors influence BVOC and GHG soil-litter fluxes in the central
871 Amazon. This study highlights the significant roles of soil and litter properties, as well as
872 microbial biomass, in driving these fluxes, with distinct patterns observed across forest types.
873 Given the complexity of the mechanisms influencing BVOC and GHG fluxes, future studies
874 should prioritize microbial activity and diversity, along with diurnal and seasonal cycles, to
875 better identify the key drivers of emission and consumption in these diverse forest ecosystems. In
876 addition, it is important to note that this research serves as a pilot study aimed at scoping out
877 general trends, and many sampling issues can be addressed in future work. For instance, utilizing
878 a PTR-ToF-MS could alleviate the challenges associated with measuring acetaldehyde, DMS,
879 and m/z 42. Longer sampling periods, ideally continuous, would allow for capturing daily
880 variations in emissions.

881 Surprisingly, despite being the least fertile and diverse forest type, the White Sand Forest
882 exhibited the highest uptake and emission fluxes. This is likely due to intrinsic environmental
883 factors, such as soil temperature and moisture, influencing microbial activity and gas fluxes, as
884 well as the unique vegetation composition of this ecosystem. Furthermore, external factors, such
885 as the preceding rainfall event, may have contributed to very high emissions, potentially
886 reflecting short-term post-rainfall pulses that would have a low or moderate effect when
887 averaged over longer periods that capture the full range of environmental conditions in these
888 ecosystems. Therefore, future studies extending the measurement duration would provide a
889 clearer understanding of how rainfall events influence average soil BVOC emissions. Finally,
890 despite their limited spatial extent in Amazonia, White Sand Forests warrant further research to
891 elucidate their ecological processes and their influence on atmospheric dynamics. Their high
892 BVOC fluxes may substantially affect key physical and chemical processes in the atmosphere,
893 with potential implications for the climate system.

894

895 **Code and Data availability**

896 All data supporting the findings of this study are available in a public repository.

897 Pinheiro de Oliveira, D., van Asperen, H., Garcia Caetano, M., Robin, M., Edtbauer, A.,
898 Zannoni, N., Byron, J., Williams, J., Demarchi, L. O., Piedade, M. T. F., Schongart, J.,
899 Wittmann, F., Júnior, S. D., Estefani Batista, C., Souza, R. A. F. de, & Alves, E. G. (2026).
900 Biogenic Volatile Organic Compounds (BVOC) and methane fluxes, microbial biomass,
901 physical and chemical properties of the soil-litter compartment across three forest types in
902 central Amazonia (2021-2022) [Data set]. Max Planck Institute for Biogeochemistry, Jena,
903 Germany. <https://doi.org/10.17871/ATTO.651.6.2645>

904 **Authors' contributions**

905 Débora Pinheiro Oliveira, Hella van Asperen, and Eliane Gomes Alves contributed to the
906 development and design of the study, as well as the collection, processing, and statistical analysis
907 of the datasets. Murielli Garcia Caetano and Michelle Robin contributed to field data collection
908 and data analysis. Achim Edtbauer helped design the methodology used in the PTR-QMS and
909 contributed to its calibration improvement. Nora Zannoni, Joseph Byron, Jonathan Williams,
910 Sergio Duvoisin-Junior, and Carla Batista contributed to the chemical analysis of BVOC samples
911 with the GC-TOF-MS and GC-MS. Layon Demarchi and Maria T. F. Piedade contributed to the
912 data analysis of the White Sand Forest. Maria T. F. Piedade, Jochen Schöngart, and Florian
913 Wittmann contributed to the dataset for the initial selection of the points in the PELD-MAUA
914 project plots where the soil chambers were installed. Rodrigo Augusto Ferreira de Souza
915 contributed to the development of the study. All authors contributed to the writing of the
916 manuscript.

917 **Competing interests**

918 The authors declare that they have no conflict of interest.

919 **Acknowledgments**

920 We thank the National Institute for Amazonian Research (INPA) and the Max Planck Institute
921 for Biogeochemistry (MPI-BGC) for their ongoing support. We would also like to thank the field
922 assistants, Jose Raimundo Ferreira Nunes and Sipko Bulthuis; and all the people involved in the
923 logistical support of the ATTO project (André Almeida, Delano Campos, Amaury Rodrigues,
924 Nagib Alberto, Valmir and Antonio Huxley), especially Roberta de Souza, who were essential to
925 the development of this study. We also thank the technicians and assistants at INPA's soil
926 laboratories - LTSP and Routine Measurements & Analyses Lab (RoMA, MPI-BGC) for their
927 valuable lab analyses. We sincerely thank Carlos Alberto Quesada for his contributions and
928 knowledge to this study. We also thank all the indigenous communities that have been bravely
929 protecting the Amazon Forest and the people from riverside communities who have always
930 worked together with us. Without the “mateiros”, we would never have achieved our scientific
931 goals.

932 **Financial support**

933 This research was supported by the National Institute for Amazonian Research (INPA), the Max
934 Planck Institute for Biogeochemistry (MPI-BGC), and the ATTO project funded by the German
935 Federal Ministry of Education and Research (BMBF grants 01LB1001A, 01LK1602,
936 01LK2101), the Brazilian Ministry of Science, Technology, Innovation and Communications
937 (contract FINEP/MCTIC 01.11.01248.00), the Amazonas State University (UEA), the Amazonas
938 Research Foundation (FAPEAM), LBA/INPA, and SDS/CEUC/RDS-Uatumã. Additional
939 support was provided by the Deutsche Forschungsgemeinschaft (DFG project 352322796) and
940 the PELD-MAUA project funded by CNPq/MCTI/CONFAP-FAPs (grant numbers
941 441811/2020-5 and 01.02.016301.02630/2022-76). D.P. Oliveira was supported by the
942 Coordination for the Improvement of Higher Education Personnel (CAPES), Brazilian Ministry
943 of Education.

944 **References**

945 Aaltonen, H., Pumpanen, J., Pihlatie, M., Hakola, H., Hellen, H., Kulmala, L., Vesala, T.,
946 and Bäck, J.: Boreal pine forest floor biogenic volatile organic compound emissions peak in
947 early summer and autumn, *Agric. For. Meteorol.*, 151, 682–691,
948 doi:10.1016/j.agrformet.2010.12.010, 2011

949 Abis, L., Loubet, B., Ciuraru, R., Lafouge, F., Houot, S., Nowak, V., Tripied, J., Dequiedt,
950 S., Maron, P. A., and Sadet-Bourgeteau, S.: Reduced microbial diversity induces larger
951 volatile organic compound emissions from soils. *Scientific Reports*, 10(1), 1–15.
952 <https://doi.org/10.1038/s41598-020-63091-8>, 2020

953 Adeney, J. M., Christensen, N. L., Vicentini, A., and Cohn-Haft, M.: White-sand
954 Ecosystems in Amazonia. *Biotropica*, 48(1), 7–23. <https://doi.org/10.1111/btp.12293>, 2016

955 Alves, E. G., Jardine, K., Tota, J., Jardine, A., Yáñez-Serrano, A. M., Karl, T., Tavares, J.,
956 Nelson, B., Gu, D., Stavrakou, T., Martin, S., Artaxo, P., Manzi, A., and Guenther, A.:
957 Seasonality of isoprenoid emissions from a primary rainforest in central Amazonia, *Atmos.*
958 *Chem. Phys.*, 16, 3903–3925, <https://doi.org/10.5194/acp-16-3903-2016>, 2016.

959 Anderson, J.M. and Ingram, J.I.S. *Tropical Soil Biology and Fertility: A Handbook of*
960 *Methods*. 2nd Edition, C.A.B. International, Wallingford, UK, 221 pp., DOI:
961 10.2307/2261129, 1993.

962 Andreae, M. O., Acevedo, O. C., Araújo, A., Artaxo, P., Barbosa, C. G. G., Barbosa, H. M.
963 J., Brito, J., Carbone, S., Chi, X., Cintra, B. B. L., da Silva, N. F., Dias, N. L., Dias-Júnior,
964 C. Q., Ditas, F., Ditz, R., Godoi, A. F. L., Godoi, R. H. M., Heimann, M., Hoffmann, T.,
965 and Yáñez-Serrano, A. M.: The Amazon Tall Tower Observatory (ATTO) in the remote
966 Amazon Basin: overview of first results from ecosystem ecology, meteorology, trace gas,
967 and aerosol measurements. *Atmospheric Chemistry and Physics Discussions*, 15(8), 11599–
968 11726. <https://doi.org/10.5194/acpd-15-11599-2015>, 2015

969 Asensio, D., Owen, S. M., Llusà, J., and Peñuelas, J.: The distribution of volatile
970 isoprenoids in the soil horizons around *Pinus halepensis* trees. *Soil Biology and*
971 *Biochemistry*, 40(12), 2937–2947. <https://doi.org/10.1016/j.soilbio.2008.08.008>, 2008

972 Asensio, D., Peñuelas, J., Llusà, J., Ogaya, R., & Filella, I. Interannual and interseasonal
973 soil CO₂ efflux and VOC exchange rates in a Mediterranean holm oak forest in response to
974 experimental drought. *Soil Biology and Biochemistry*, 39(10), 2471-2484.
975 <https://doi.org/10.1016/j.soilbio.2007.04.019>, 2007.

976 Bach, T. J., and Rohmer, M.: Isoprenoid synthesis in plants and microorganisms: new

977 concepts and experimental approaches, Springer, doi:10.1007/978-1-4614-4063-5, 2013.

978 Baggesen, N. S., Davie-Martin, C. L., Seco, R., Holst, T., and Rinnan, R. Bidirectional
979 Exchange of Biogenic Volatile Organic Compounds in Subarctic Heath Mesocosms During
980 Autumn Climate Scenarios. *Journal of Geophysical Research: Biogeosciences*, 127(6).
981 <https://doi.org/10.1029/2021JG006688>, 2022.

982 Beauchamp, J., Herbig, J., Gutmann, R. and Hansel, A. On the use of Tedlar bags for
983 breath-gas sampling and analysis, *J. Breath Res.*, 2, 046001, doi:10.1088/1752-
984 7155/2/4/046001, 2008.

985 Borges, S. H., Whittaker, A., and de Almeida, R. A. M.: Bird diversity in the Serra do Aracá
986 region, northwestern Brazilian Amazon: Preliminary check-list with considerations on
987 biogeography and conservation. *Zoologia*, 31, 343–360, [https://doi.org/10.1590/S1984-](https://doi.org/10.1590/S1984-46702014000400006)
988 [46702014000400006](https://doi.org/10.1590/S1984-46702014000400006), 2014

989 Botía, S., Komiya, S., Marshall, J., Koch, T., Gałkowski, M., Lavric, J., Gomes-Alves, E.,
990 Walter, D., Fisch, G., Pinho, D. M., Nelson, B. W., Martins, G., Luijckx, I. T., Koren, G.,
991 Florentie, L., Carioca de Araújo, A., Sá, M., Andreae, M. O., Heimann, M., and Gerbig, C.:
992 The CO₂ record at the Amazon Tall Tower Observatory: A new opportunity to study
993 processes on seasonal and inter-annual scales. *Global Change Biology*, 28(2), 588–611.
994 <https://doi.org/10.1111/gcb.15905>, 2022

995 Bourtsoukidis, E., Behrendt, T., Yañez-Serrano, A. M., Hellén, H., Diamantopoulos, E.,
996 Catão, E., Ashworth, K., Pozzer, A., Quesada, C. A., Martins, D. L., Sá, M., Araujo, A.,
997 Brito, J., Artaxo, P., Kesselmeier, J., Lelieveld, J., and Williams, J.: Strong sesquiterpene
998 emissions from Amazonian soils. *Nature Communications*, 9(1), 1–11.
999 <https://doi.org/10.1038/s41467-018-04658-y>, 2018

1000 Butterbach-Bahl K, Baggs EM, Dannenmann M, Kiese R, Zechmeister-Boltenstern S.
1001 Nitrous oxide emissions from soils: how well do we understand the processes and their
1002 controls? *Philos Trans R Soc Lond B Biol Sci*. doi: 10.1098/rstb.2013.0122, 2013.

1003 Caetano Garcia, M.: Biogenic volatile organic compound (BVOC) emissions from
1004 decomposing leaf-litter in central Amazonia (Doctoral dissertation, National Institute for

1005 Amazonian Research Manaus), 2022

1006 Carruthers, D. N., & Lee, T. S.. Diversifying Isoprenoid Platforms via Atypical Carbon
1007 Substrates and Non-model Microorganisms. *Frontiers in Microbiology*, 12, 791089.
1008 <https://doi.org/10.3389/fmicb.2021.791089>, 2021

1009 Chambers, J.Q., Tribuzy, E.S., Toledo, L.C., Crispim, B.F., Higuchi, N., Santos, J.d.,
1010 Araújo, A.C., Kruijt, B., Nobre, A.D. and Trumbore, S.E. RESPIRATION FROM A
1011 TROPICAL FOREST ECOSYSTEM: PARTITIONING OF SOURCES AND LOW
1012 CARBON USE EFFICIENCY. *Ecological Applications*, 14: 72-88.
1013 <https://doi.org/10.1890/01-6012>, 2004

1014 Chomel, M., Guittonny-Larchevêque, M., Fernandez, C., Gallet, C., DesRochers, A., Paré,
1015 D., Jackson, B. G., and Baldy, V.: Plant secondary metabolites: A key driver of litter
1016 decomposition and soil nutrient cycling. *J. Ecol.*, 104, 1527–1541,
1017 <https://doi.org/10.1111/1365-2745.12644>, 2016

1018 Conrad, R: Methane production in soil environments— anaerobic biogeochemistry and
1019 microbial life between flooding and desiccation. *Microorganisms*, 8(6), 1–12.
1020 <https://doi.org/10.3390/microorganisms8060881>, 2020.

1021 Conrad, R: The global methane cycle: Recent advances in understanding the microbial
1022 processes involved. *Environmental Microbiology Reports*, 1(5), 285–292.
1023 <https://doi.org/10.1111/j.1758-2229.2009.00038.x>, 2009.

1024 Cornu, S., Ambrosi, J. P., Lucas, Y., and Fevrier, D.: A comparative study of the soil
1025 solution chemistry of two Amazonian forest soils (Central Amazonia, Brazil). In *Hydrology*
1026 *and Earth System Sciences* (Vol. 1, Issue 2, pp. 313–324). [https://doi.org/10.5194/hess-1-](https://doi.org/10.5194/hess-1-313-1997)
1027 [313-1997](https://doi.org/10.5194/hess-1-313-1997), 1997

1028 Costa, F. R. C., Schietti, J., Stark, S. C., and Smith, M. N.: The other side of tropical forest
1029 drought: do shallow water table regions of Amazonia act as large-scale hydrological refugia
1030 from drought? *New Phytologist*, 237(3), 714–733. <https://doi.org/10.1111/nph.17914>, 2023

1031 Crocker, L., Guo, J., U'Ren, J. M., Pugliese, G., Ladd, S. N., Werner, C., & Meredith, L. K.

1032 Volatile organic compound (VOC) exchange in tropical leaf litter in response to wetting:
1033 An automated scheme to classify flux pulse dynamics. *Journal of Geophysical Research:*
1034 *Biogeosciences*, 130, e2025JG008774. <https://doi.org/10.1029/2025JG008774>, 2025.

1035 de Mendonça, B. A. F., Filho, E. I. F., Schaefer, C. E. G. R., Simas, F. N. B., and de Paula,
1036 M. D.: Os solos das campinaranas na amazônia Brasileira: Ecossistemas arenícolas
1037 oligotróficos. *Ciencia Florestal*, 25(4), 827–839. <https://doi.org/10.5902/1980509820581>,
1038 2015

1039 Demarchi, L. O., Klein, V. P., Aguiar, D. P. P., Marinho, L. C., Ferreira, M. J., Lopes, A.,
1040 da Cruz, J., Quaresma, A. C., Schöngart, J., Wittmann, F., and Piedade, M. T. F.: The
1041 specialized white-sand flora of the Uatumã Sustainable Development Reserve, central
1042 Amazon, Brazil, *Check List*, 18, 187–217, <https://doi.org/10.15560/18.1.187>, 2022

1043 Draper, F. C., Roucoux, K. H., Lawson, I. T., Mitchard, E. T. A., Honorio Coronado, E. N.,
1044 Lähteenoja, O., Montenegro, L. T., Sandoval, E. V., Zaráte, R., and Baker, T. R.: The
1045 distribution and amount of carbon in the largest peatland complex in Amazonia, *Environ.*
1046 *Res. Lett.*, 9, 124017, <https://doi.org/10.1088/1748-9326/9/12/124017>, 2014.

1047 Drewer, J., Leduning, M. M., Purser, G., Cash, J. M., Sentian, J., and Skiba, U. M.:
1048 Monoterpenes from tropical forest and oil palm plantation floor in Malaysian
1049 Borneo/Sabah: emission and composition, *Environ. Sci. Pollut. Res.*, 28, 31792–31802, doi:
1050 10.1007/s11356-021-13052-z., 2021.

1051 Dunne, E., Galbally, I. E., Lawson, S., and Patti, A.: Interference in the PTR-MS
1052 measurement of acetonitrile at m/z 42 in polluted urban air—a study using switchable
1053 reagent ion PTR-MS, *Int. J. Mass Spectrom.*, 319–320, 40–47,
1054 <https://doi.org/10.1016/j.ijms.2012.05.004>, 2012

1055 Doff sotta, E., Meir, P., Malhi, Y., Donato nobre, A., Hodnett, M. and Grace, J. Soil CO₂
1056 efflux in a tropical forest in the central Amazon. *Global Change Biology*, 10: 601-617.
1057 <https://doi.org/10.1111/j.1529-8817.2003.00761.x>, 2004

1058 Edtbauer, A., Pfannerstill, E. Y., Pires Florentino, A. P., Barbosa, C. G. G., Rodriguez-
1059 Caballero, E., Zannoni, N., Alves, R. P., Wolff, S., Tsokankunku, A., Aptroot, A., de

1060 Oliveira Sá, M., de Araújo, A. C., Sörgel, M., de Oliveira, S. M., Weber, B., and Williams,
1061 J.: Cryptogamic organisms are a substantial source and sink for volatile organic compounds
1062 in the Amazon region, *Commun. Earth Environ.*, 2, 1–10, [https://doi.org/10.1038/s43247-](https://doi.org/10.1038/s43247-021-00328-y)
1063 021-00328-y, 2021

1064 Steeghs, M., Bais, H. P., de Gouw, J., Goldan, P., Kuster, W., Northway, M., Fall, R., and
1065 Vivanco, J. M.: Proton-transfer-reaction mass spectrometry as a new tool for real time
1066 analysis of root-secreted volatile organic compounds in *Arabidopsis*, *Plant Physiol.*, 135,
1067 47–58, <https://doi.org/10.1104/pp.104.038703>, 2004

1068 Emidio, K., Martins, S. V., Antônio, C., and Soares, A.: Structure of 15 hectares permanent
1069 plots of terra firme dense forest in central Amazon, 01, 603–615,
1070 <https://doi.org/10.1590/0100-67622016000400004>, 2016.

1071 Empresa Brasileira de Pesquisa Agropecuária. Manual de análise química de solos, plantas
1072 e fertilizantes, 2nd Edn., EMBRAPA, Brasília, 1999.

1073 Eyice, Ö., Namura, M., Chen, Y., McGenity, T. J., and Murrell, J. C.: SIP metagenomics
1074 identifies uncultivated Methylophilaceae as dimethylsulphide degrading bacteria in soil and
1075 lake sediment, *ISME J.*, 9, 2336–2348, <https://doi.org/10.1038/ismej.2015.37>, 2015

1076 Fan, J., Luo, R., McConkey, B. G., and Ziadi, N.: Effects of nitrogen deposition and litter
1077 layer management on soil CO₂, N₂O, and CH₄ emissions in a subtropical pine forestland,
1078 *Sci. Rep.*, 10, 1–11, <https://doi.org/10.1038/s41598-020-65952-8>, 2020

1079 Fan, Y., Zhang, Y., Osborne, B., and Zou, J.: Global patterns of soil greenhouse gas fluxes
1080 in response to litter manipulation, *Cell Rep. Sustain.*, 1, 100003,
1081 <https://doi.org/10.1016/j.crsus.2023.100003>, 2024.

1082 Fine, P. V. A, Mesones, I., & Coley, P. D. Herbivores promote habitat specialization by
1083 trees in amazonian forests. *Science*. <https://doi.org/3050663>, 2004.

1084 Fine, P. V. A., and Baraloto, C.: Habitat endemism in white-sand forests: insights into the
1085 mechanisms of lineage diversification and community assembly of the Neotropical flora,
1086 *Biotropica*, 48, 24–33, <https://doi.org/10.1111/btp.12301>, 2016.

1087 Fine, P. V. A., Miller, Z. J., Mesones, I., Irazuzta, S., Appel, H. M., Stevens, M. H. H.,
1088 Sääksjärvi, I., Schultz, J. C., and Coley, P. D.: The growth-defense trade-off and habitat
1089 specialization by plants in Amazonian forests, *Ecology*, 87, 150–162,
1090 <https://doi.org/10.1126/science.1098982>, 2006

1091 Flint, A. L., and Flint, L. E.: Particle density, in: *Methods of Soil Analysis, Part 4: Physical*
1092 *Methods*, 229–240. <https://doi.org/10.2136/sssabookser5.4.c10>, 2002.

1093 Franco, W., and Dezzeo, N.: Soils and soil-water regime in the terra-firme-caatinga forest
1094 complex near San Carlos de Rio Negro, state of Amazonas, Venezuela, *Interciencia*, 19,
1095 305–316, 1994.

1096 García-Villacorta, R., Dexter, K. G., and Pennington, T.: Amazonian white-sand forests
1097 show strong floristic links with surrounding oligotrophic habitats and the Guiana Shield,
1098 *Biotropica*, 48, 47–57, <https://doi.org/10.1111/btp.12302>, 2016.

1099 Gfeller, A., Laloux, M., Barsics, F., Kati, D. E., Haubruge, E., du Jardin, P., Verheggen, F.
1100 J., Lognay, G., Wathelet, J. P., and Fauconnier, M. L.: Characterization of volatile organic
1101 compounds emitted by barley (*Hordeum vulgare* L.) roots and their attractiveness to
1102 wireworms, *J. Chem. Ecol.*, 39, 1129–1139, <https://doi.org/10.1007/s10886-013-0302-3>,
1103 2013

1104 Gomes Alves, E., Taylor, T., Robin, M., Pinheiro Oliveira, D., Schietti, J., Duvoisin Júnior,
1105 S., Zannoni, N., Williams, J., Hartmann, C., Gonçalves, J. F. C., Schöngart, J., Wittmann,
1106 F., and Piedade, M. T. F.: Seasonal shifts in isoprenoid emission composition from three
1107 hyperdominant tree species in central Amazonia, *Plant Biol.*, 24, 721–733, Seasonal shifts
1108 in isoprenoid emission composition from three hyperdominant tree species in central
1109 Amazonia. *Plant Biology*, 24(5), 721–733. <https://doi.org/10.1111/plb.13419>, 2022

1110 Greenberg, J. P., Asensio, D., Turnipseed, A., Guenther, A. B., Karl, T., and Gochis, D.:
1111 Contribution of leaf and needle litter to whole ecosystem BVOC fluxes, *Atmos. Environ.*,
1112 59, 302–311, <https://doi.org/10.1016/j.atmosenv.2012.04.038>, 2012.

1113 Guenther, A. B., Jiang, X., Heald, C. L., Sakulyanontvittaya, T., Duhl, T., Emmons, L. K.,
1114 and Wang, X.: The model of emissions of gases and aerosols from nature version 2.1

1115 (MEGAN2.1): an extended and updated framework for modeling biogenic emissions,
1116 Geosci. Model Dev., 5, 1471–1492, <https://doi.org/10.5194/gmd-5-1471-2012>.

1117 Hair, J. F., Black, W. C., Babin, B. J. and Anderson, R. E. Multivariate data analysis, 7th
1118 Edn., Pearson, Upper Saddle River, 2009.

1119 Hebbali, A. (2024). Olsrr: Tools for building OLS regression models.

1120 Hernandez-Arranz, S., Perez-Gil, J., Marshall-Sabey, D., and Rodriguez-Concepcion, M.:
1121 Engineering *Pseudomonas putida* for isoprenoid production by manipulating endogenous
1122 and shunt pathways supplying precursors, *Microb. Cell Fact.*, 18, 1–14,
1123 <https://doi.org/10.1186/s12934-019-1204-z>, 2019

1124 Hernandez, L.K., Pugliese, G., Ingrisch, J. et al. Drought re-routes soil microbial carbon
1125 metabolism towards emission of volatile metabolites in an artificial tropical rainforest. *Nat*
1126 *Microbiol* 8, 1480–1494. <https://doi.org/10.1038/s41564-023-01432-9>, 2023.

1127 Hofmann, K., Pauli, H., Praeg, N., Wagner, A. O., and Illmer, P.: Methane-cycling
1128 microorganisms in soils of a high-alpine altitudinal gradient, *FEMS Microbiol. Ecol.*, 92,
1129 *fiw009*, <https://doi.org/10.1093/femsec/fiw009>, 2016

1130 Huangfu, Y., Yuan, B., Wang, S., Wu, C., He, X., Qi, J., de Gouw, J., Warneke, C., Gilman,
1131 J. B., Wisthaler, A., Karl, T., Graus, M., Jobson, B. T., and Shao, M.: Revisiting acetonitrile
1132 as tracer of biomass burning in anthropogenic-influenced environments, *Geophys. Res.*
1133 *Lett.*, 48, e2020GL092322, <https://doi.org/10.1029/2020GL092322>, 2021

1134 Jardine, K., Yáñez-Serrano, A. M., Williams, J., Kunert, N., Jardine, A., Taylor, T., Abrell,
1135 L., et al.: Dimethyl sulfide in the Amazon rainforest, *Glob. Biogeochem. Cycles*, 29, 19–32,
1136 <https://doi.org/10.1002/2014GB004969>, 2015

1137 Jdanova, M., and Isidorov, V.: Volatile organic compounds from leaves litter,
1138 *Chemosphere*, 48, 2058–2072, doi:10.1016/S0045-6535(02)00365-7, 2002.

1139 Jenkinson, D. S., Brookes, P. C., and Powlson, D. S.: Measuring soil microbial biomass,
1140 *Soil Biol. Biochem.*, 36, 5–7, <https://doi.org/10.1016/j.soilbio.2003.10.002>, 2004

1141 Jiao, Y., Kramshøj, M., Davie-Martin, C. L., Albers, C. N., and Rinnan, R.: Soil uptake of
1142 VOCs exceeds production when VOCs are readily available, *Soil Biol. Biochem.*, 185,
1143 109153, <https://doi.org/10.1016/j.soilbio.2023.109153>, 2023

1144 Kesselmeier, J., & Hubert, A. Exchange of reduced volatile sulfur compounds between leaf
1145 litter and the atmosphere. *Atmospheric Environment*, 36(29), 4679-4686.
1146 [https://doi.org/10.1016/S1352-2310\(02\)00413-2](https://doi.org/10.1016/S1352-2310(02)00413-2), 2002.

1147 Kuzma, J., Nemecek-Marshall, M., Pollock, W. H., and Fall, R.: Bacteria produce the
1148 volatile hydrocarbon isoprene, *Curr. Microbiol.*, 30, 97–103,
1149 <https://doi.org/10.1007/BF00294190>, 1995

1150 Lange, D.F., Schröter, S.A., da Luz, F.M. et al. Cycling of dissolved organic nutrients and
1151 indications for nutrient limitations in contrasting Amazon rainforest ecosystems.
1152 *Biogeochemistry* 167, 1567–1588. <https://doi.org/10.1007/s10533-024-01187-3>, 2024.

1153 Lee, J., Oh, Y., Lee, S. T., Seo, Y. O., Yun, J., Yang, Y., Kim, J., Zhuang, Q., and Kang, H.:
1154 Soil organic carbon is a key determinant of CH₄ sink in global forest soils, *Nat. Commun.*,
1155 14, 6–13, <https://doi.org/10.1038/s41467-023-38905-8>, 2023

1156 Leff, J. W., and Fierer, N.: Volatile organic compound (VOC) emissions from soil and litter
1157 samples, *Soil Biol. Biochem.*, 40, 1629–1636, <https://doi.org/10.1016/j.soilbio.2008.01.018>,
1158 2008

1159 Lehnert, A. S., Cooper, R. E., Ignatz, R., Ruecker, A., Gomes-Alves, E., Küsel, K., Pohnert,
1160 G., and Trumbore, S. E.: Dimethyl sulfide emissions from a peatland result more from
1161 organic matter degradation than sulfate reduction, *J. Geophys. Res. Biogeosci.*, 129,
1162 e2023JG007449, <https://doi.org/10.1029/2023JG007449>, 2024

1163 Li Q, Hu W, Li L, Li Y. Interactions between organic matter and Fe oxides at soil micro-
1164 interfaces: Quantification, associations, and influencing factors. *Sci Total Environ.*
1165 10;855:158710. doi: 10.1016/j.scitotenv.2022.158710, 2023.

1166 Lin, C., Owen, S. M., and Peñuelas, J.: Volatile organic compounds in the roots and
1167 rhizosphere of *Pinus* spp., *Soil Biol. Biochem.*, 39, 951–960,

1168 <https://doi.org/10.1016/j.soilbio.2006.11.007>, 2007

1169 Lindinger, W., Hansel, A., and Jordan, A.: On-line monitoring of volatile organic
1170 compounds at pptv levels by means of proton-transfer-reaction mass spectrometry (PTR-
1171 MS) medical applications, food control and environmental research, *Int. J. Mass Spectrom.*
1172 *Ion Process.*, 173, 191–241, [https://doi.org/10.1016/s0168-1176\(97\)00281-4](https://doi.org/10.1016/s0168-1176(97)00281-4), 1998

1173 Liu, M., and Matsui, H.: Secondary organic aerosol formation regulates cloud condensation
1174 nuclei in the global remote troposphere, *Geophys. Res. Lett.*, 49,
1175 e2022GL100543,<https://doi.org/10.1029/2022GL100543>, 2022.

1176 Liu, Y., Ciuraru, R., Abis, L., Amelynck, C., Buysse, P., Guenther, A., Heinesch, B.,
1177 Lafouge, F., Levavasseur, F., Loubet, B., Voyard, A., and Massad, R.-S.: Emissions of
1178 biogenic volatile organic compounds from agricultural lands and the impact of land-use and
1179 other management practices: a review, *EGUsphere* [preprint], 1–35,
1180 <https://doi.org/10.5194/egusphere-2024-530>, 2024

1181 Llusia, J., Asensio, D., Sardans, J., Filella, I., Peguero, G., Grau, O., Ogaya, R., Gargallo-
1182 Garriga, A., Verryckt, L. T., Van Langenhove, L., Brechet, L. M., Courtois, E., Stahl, C.,
1183 Janssens, I. A., and Peñuelas, J.: Contrasting nitrogen and phosphorus fertilization effects
1184 on soil terpene exchanges in a tropical forest, *Sci. Total Environ.*, 802,
1185 149769,<https://doi.org/10.1016/j.scitotenv.2021.149769>, 2022

1186 Luize, B. G., Magalhães, J. L. L., Queiroz, H., Lopes, M. A., Venticinque, E. M., de Moraes
1187 Novo, E. M. L., and Silva, T. S. F.: The tree species pool of Amazonian wetland forests:
1188 which species can assemble in periodically waterlogged habitats?, *PLoS ONE*, 13,
1189 e0198130, <https://doi.org/10.1371/journal.pone.0198130>, 2018

1190 Mäki, M., Heinonsalo, J., Hellén, H., and Bäck, J.: Contribution of understorey vegetation
1191 and soil processes to boreal forest isoprenoid exchange, *Biogeosciences*, 14, 1055–1073,
1192 <https://doi.org/10.5194/bg-14-1055-2017>, 2017

1193 Malavolta, E., Vitti, G.C. and Oliveira, S.A. Avaliação do estadonutricional das plantas:
1194 Princípios e aplicações. [Evaluation of the Nutritional Status of Plants: Principles and
1195 Applications.] Piracicaba, Potafos, 321 pp., 1989.

1196 Mancuso, S., Taiti, C., Bazihizina, N., Costa, C., Menesatti, P., Giagnoni, L., Arenella, M.,
1197 Nannipieri, P., and Renella, G.: Soil volatile analysis by proton transfer reaction-time of
1198 flight mass spectrometry (PTR-TOF-MS), *Appl. Soil Ecol.*, 86, 182–191,
1199 <https://doi.org/10.1016/j.apsoil.2014.10.018>, 2015

1200 Mazahar, S., and Umar, S.: Soil potassium availability and role of microorganisms in
1201 influencing potassium availability to plants, in: *Role of potassium in abiotic stress*, 77–87,
1202 https://doi.org/10.1007/978-981-16-4461-0_4, 2022

1203 McGenity, T. J., Crombie, A. T., and Murrell, J. C.: Microbial cycling of isoprene, the most
1204 abundantly produced biological volatile organic compound on Earth, *ISME J.*, 12, 931–941,
1205 <https://doi.org/10.1038/s41396-018-0072-6>, 2018

1206 Miyama, T., Morishita, T., Kominami, Y., Noguchi, H., Yasuda, Y., Yoshifuji, N., Okano,
1207 M., Yamanoi, K., Mizoguchi, Y., Takanashi, S., Kitamura, K., and Matsumoto, K.:
1208 Increases in biogenic volatile organic compound concentrations observed after rains at six
1209 forest sites in non-summer periods, *Atmosphere*, 11, 13181,
1210 <https://doi.org/10.3390/atmos11121381>, 2020

1211 Monard, C., Caudal, J. P., Cluzeau, D., Le Garrec, J. L., Hellequin, E., Hoeffner, K.,
1212 Humbert, G., Jung, V., Le Lann, C., and Nicolai, A.: Short-term temporal dynamics of VOC
1213 emissions by soil systems in different biotopes, *Front. Environ. Sci.*, 9, 650701,
1214 <https://doi.org/10.3389/fenvs.2021.650701>, 2021

1215 Mosquera, Q. H.; Torres-Torres, J.J.; Pérez-Abadía, D. Influence of Mining on Nutrient
1216 Cycling in the Tropical Rain Forests of the Colombian Pacific. *Forests* 2024, 15, 1222.
1217 <https://doi.org/10.3390/f15071222>

1218 Murphy, J., and Riley, J. P.: A modified single solution method for the determination of
1219 phosphate in natural waters, *Anal. Chim. Acta*, 27, 31–36, [https://doi.org/10.1016/S0003-](https://doi.org/10.1016/S0003-2670(00)88444-5)
1220 [2670\(00\)88444-5](https://doi.org/10.1016/S0003-2670(00)88444-5), 1962

1221 Murrell, J. C., McGenity, T. J., and Crombie, A. T.: Microbial metabolism of isoprene: a
1222 much-neglected climate-active gas, *Microbiology*, 166, 600–613,
1223 <https://doi.org/10.1099/mic.0.000931>, 2020

1224 Ndah, F., Valolahti, H., Schollert, M., Michelsen, A., and Kivimäenpää, M.: Influence of
1225 increased nutrient availability on biogenic volatile organic compound (BVOC) emissions
1226 and leaf anatomy of subarctic dwarf shrubs under climate warming and increased
1227 cloudiness, *Ann. Bot.*, 129, 443–455, doi:10.1093/aob/mcac004, 2022.

1228 Oliveira-Filho, A. T., Dexter, K. G., Pennington, R. T., Simon, M. F., Bueno, M. L., and
1229 Neves, D. M.: On the floristic identity of Amazonian vegetation types, *Biotropica*, 53, 767–
1230 777, <https://doi.org/10.1093/aob/mcac004>, 2021

1231 Olsen, S.R. and Sommers, L.E. Phosphorus. In: Page, A.L., Ed., *Methods of Soil Analysis*
1232 *Part 2 Chemical and Microbiological Properties*, American Society of Agronomy, Soil
1233 Science Society of America, Madison, 403-430, 1982.

1234 Package, T. *olsrr: tools for building OLS regression models*, R package version 0.5.3,
1235 <cran.r-project.org>, 2024.

1236 Peñuelas, J., Asensio, D., Tholl, D., Wenke, K., Rosenkranz, M., Piechulla, B., and
1237 Schnitzler, J. P.: Biogenic volatile emissions from the soil, *Plant Cell Environ.*, 37, 1866–
1238 1891, <https://doi.org/10.1111/pce.12340>, 2014.

1239 Pohlman, J. W., Casso, M., Magen, C., and Bergeron, E.: Discrete Sample Introduction
1240 Module for Quantitative and Isotopic Analysis of Methane and Other Gases by Cavity
1241 Ring-Down Spectroscopy, *Environ. Sci. Technol.*, 55, 12066–12074,
1242 <https://doi.org/10.1021/acs.est.1c01386>, 2021.

1243 Pugliese, G., Ingrisch, J., Meredith, L. K., Pfannerstill, E. Y., Klüpfel, T., Meeran, K.,
1244 Byron, J., Purser, G., Gil-Loaiza, J., van Haren, J., Dontsova, K., Kreuzwieser, J., Ladd, S.
1245 N., Werner, C., and Williams, J.: Effects of drought and recovery on soil volatile organic
1246 compound fluxes in an experimental rainforest, *Nat. Commun.*, 14, 40661,
1247 <https://doi.org/10.1038/s41467-023-40661-8>, 2023

1248 Pulido, P., Perello, C., and Rodriguez-Concepcion, M.: New insights into plant isoprenoid
1249 metabolism, *Mol. Plant*, 5, 964–967, <https://doi.org/10.1093/mp/sss088>, 2012

1250 Quesada, C. A., Lloyd, J., Anderson, L. O., Fyllas, N. M., Schwarz, M., and Czimeczik, C.

1251 I.: Soils of Amazonia with particular reference to the RAINFOR sites, *Biogeosciences*, 8,
1252 1415–1440, <https://doi.org/10.5194/bg-8-1415-2011>, 2011

1253 Quesada, C. A., Lloyd, J., Schwarz, M., Baker, T. R., Phillips, O. L., Patiño, S., Czimczik,
1254 C., Hodnett, M. G., Herrera, R., Arneth, A., Lloyd, G., Malhi, Y., Dezzeo, N., Luizão, F. J.,
1255 Santos, A. J. B., Schmerler, J., Arroyo, L., Silveira, M., Priante Filho, N., and Ramírez, H.:
1256 Regional and large-scale patterns in Amazon forest structure and function are mediated by
1257 variations in soil physical and chemical properties, *Biogeosciences Discuss.*, 6, 3993–4057,
1258 <https://doi.org/10.5194/bgd-6-3993-2009>, 2009

1259 Quesada, C. A., Phillips, O. L., Schwarz, M., Czimczik, C. I., Baker, T. R., Patiño, S.,
1260 Fyllas, N. M., Hodnett, M. G., Herrera, R., Almeida, S., Alvarez Dávila, E., Arneth, A.,
1261 Arroyo, L., Chao, K. J., Dezzeo, N., Erwin, T., Di Fiore, A., Higuchi, N., Honorio
1262 Coronado, E., and Lloyd, J.: Basin-wide variations in Amazon forest structure and function
1263 are mediated by both soils and climate, *Biogeosciences*, 9, 2203–2246,
1264 <https://doi.org/10.5194/bg-9-2203-2012>.

1265 Raio, A., Brillì, F., Baraldi, R., Neri, L., & Puopolo, G. Impact of spontaneous mutations on
1266 physiological traits and biocontrol activity of *Pseudomonas chlororaphis* M71.
1267 *Microbiological Research*, 239, 126517. <https://doi.org/10.1016/j.micres.2020.126517,2020>.

1268 Rasheed, M. U., Kivimäenpää, M., and Kasurinen, A.: Emissions of biogenic volatile
1269 organic compounds (BVOCs) from the rhizosphere of Scots pine (*Pinus sylvestris*)
1270 seedlings exposed to warming, moderate N addition and bark herbivory by large pine
1271 weevil (*Hylobius abietis*), *Plant Soil*, 463, 379–394, [https://doi.org/10.1007/s11104-021-](https://doi.org/10.1007/s11104-021-04888-y)
1272 04888-y, 2021

1273 Raza, W., Mei, X., Wei, Z., Ling, N., Yuan, J., Wang, J., Huang, Q., and Shen, Q.: Profiling
1274 of soil volatile organic compounds after long-term application of inorganic, organic and
1275 organic-inorganic mixed fertilizers and their effect on plant growth, *Sci. Total Environ.*,
1276 607–608, 326–338, <https://doi.org/10.1016/j.scitotenv.2017.07.023>, 2017

1277 Rodrigues, Julia & Martins, Walmer & de Oliveira, Victor & Wanzerley, Myriam &
1278 Pacheco, Hiago & Menezes, Felipe & Oliveira, Francisco. Litter stock, litterfall and

1279 nutrients in the Amazonia: defining patterns from last 40 years of scientific research.
1280 Scientia Plena. 19. 10.14808/sci.plena.2023.077301, 2023.

1281 Rossetti, D. F., Moulatlet, G. M., Tuomisto, H., Gribel, R., Toledo, P. M., Valeriano, M.
1282 M., Ruokolainen, K., Cohen, M. C. L., Cordeiro, C. L. O., Rennó, C. D., Coelho, L. S., and
1283 Ferreira, C. A. C.: White sand vegetation in an Amazonian lowland under the perspective of
1284 a young geological history, *An. Acad. Bras. Cienc.*, 91, e20181337,
1285 <https://doi.org/10.1590/0001-3765201920181337>, 2019

1286 Saggar, S., Jha, N., Deslippe, J., Bolan, N., Luo, J., Giltrap, D., Kim, D., Zaman, M., &
1287 Tillman, R. Denitrification and N₂O:N₂ production in temperate grasslands: Processes,
1288 measurements, modelling and mitigating negative impacts. *Science of The Total*
1289 *Environment*, 465, 173-195. <https://doi.org/10.1016/j.scitotenv.2012.11.050>, 2013.

1290 Saunier, A., Mpamah, P., Biasi, C., and Blande, J. D.: Microorganisms in the phylloplane
1291 modulate the BVOC emissions of Brassica nigra leaves, *Plant Signal. Behav.*, 15, 1728468,
1292 <https://doi.org/10.1080/15592324.2020.1728468>, 2020

1293 Schindler, T., Mander, Ü., Machacova, K., Espenberg, M., Krasnov, D., Escuer-Gatius, J.,
1294 Veber, G., Pärn, J., and Soosaar, K.: Short-term flooding increases CH₄ and N₂O emissions
1295 from trees in a riparian forest soil-stem continuum, *Sci. Rep.*, 10, 60058,
1296 <https://doi.org/10.1038/s41598-020-60058-7>, 2020

1297 Sillo, F., Neri, L., Calvo, A., Zampieri, E., Petruzzelli, G., Ferraris, I., Delledonne, M.,
1298 Zaldei, A., Gioli, B., Baraldi, R., and Balestrini, R.: Correlation between microbial
1299 communities and volatile organic compounds in an urban soil provides clues on soil quality
1300 towards sustainability of city flowerbeds, *Heliyon*, 10, e23594,
1301 <https://doi.org/10.1016/j.heliyon.2023.e23594>, 2024.

1302 Simon, C., Pimentel, T. P., Monteiro, M. T. F., Candido, L. A., Gastmans, D., Geilmann,
1303 H., ... & Gleixner, G.: Molecular links between whitesand ecosystems and blackwater
1304 formation in the Rio Negro watershed. *Geochimica et Cosmochimica Acta*, 311, 274-291.
1305 <https://doi.org/10.1016/j.gca.2021.06.036>, 2021

1306 Sindelarova, K., Granier, C., Bouarar, I., Guenther, A., Tilmes, S., Stavrakou, T., Müller, J.-

1307 F., Kuhn, U., Stefani, P., and Knorr, W.: Global data set of biogenic VOC emissions
1308 calculated by the MEGAN model over the last 30 years, *Atmos. Chem. Phys.*, 14, 9317–
1309 9341, <https://doi.org/10.5194/acp-14-9317-2014>, 2014.

1310 Snyder, C. S., Bruulsema, T. W., Jensen, T. L., and Fixen, P. E.: Review of greenhouse gas
1311 emissions from crop production systems and fertilizer management effects, *Agric. Ecosyst.*
1312 *Environ.*, 133, 247–266, <https://doi.org/10.1016/j.agee.2009.04.021> , 2009.

1313 Stotzky, G., Schenck, S., and Papavizas, G. C.: Volatile organic compounds and
1314 microorganisms, *Crit. Rev. Microbiol.*, 4, 333–382,
1315 <https://doi.org/10.3109/10408417609102303>, 1976

1316 Tang, J., Schurgers, G., and Rinnan, R.: Process understanding of soil BVOC fluxes in
1317 natural ecosystems: a review, *Rev. Geophys.*, 57, 966–986,
1318 <https://doi.org/10.1029/2018RG000634>, 2019

1319 ter Steege, H., Pitman, N. C. A., Sabatier, D., Baraloto, C., Salomão, R. P., Guevara, J. E.,
1320 Phillips, O. L., Castilho, C. V., Magnusson, W. E., Molino, J. F., Monteagudo, A., Vargas,
1321 P. N., Montero, J. C., Feldpausch, T. R., Coronado, E. N. H., Killeen, T. J., Mostacedo, B.,
1322 Vasquez, R., Assis, R. L., and Silman, M. R.: Hyperdominance in the Amazonian tree flora,
1323 *Science*, 342, 1243092, <https://doi.org/10.1126/science.1243092>, 2013

1324 Thulasiram, H. V., Erickson, H. K., and Poulter, C. D.: Chimeras of two isoprenoid
1325 synthases catalyze all four coupling reactions in isoprenoid biosynthesis, *Science*, 316, 73–
1326 76, <https://doi.org/10.1126/science.1137786>, 2007

1327 Tripathi, N., Krumm, B. E., Edtbauer, A., Spracklen, D. V., and Kanzow, T.: Impacts of
1328 convection, chemistry, and forest clearing on biogenic volatile organic compounds over the
1329 Amazon, *Nat. Commun.*, 16, 4692, <https://doi.org/10.1038/s41467-025-59953-2> , 2025.

1330 Trowbridge, A. M., Stoy, P. C., and Phillips, R. P.: Soil biogenic volatile organic compound
1331 flux in a mixed hardwood forest: net uptake at warmer temperatures and the importance of
1332 mycorrhizal associations, *J. Geophys. Res. Biogeosci.*, 125, e2019JG005479,
1333 <https://doi.org/10.1029/2019JG005479>, 2020

1334 van Asperen, H., Warneke, T., Carioca de Araújo, A., Forsberg, B., José Filgueiras Ferreira,
1335 S., Röckmann, T., van der Veen, C., Bulthuis, S., Ramos de Oliveira, L., de Lima Xavier,
1336 T., da Mata, J., de Oliveira Sá, M., Ricardo Teixeira, P., Andrews de França e Silva, J.,
1337 Trumbore, S., and Notholt, J.: The emission of CO from tropical rainforest soils,
1338 *Biogeosciences*, 21, 3183–3199, <https://doi.org/10.5194/bg-21-3183-2024>, 2024.

1339 van Asperen, H., Warneke, T., Carioca de Araújo, A., Rider Forsberg, B., Ramos de
1340 Oliveira, L., de Lima Xavier, T., de Oliveira Sá, M., Ricardo Teixeira, P., Azevedo de
1341 Oliveira, R., Sousa de Moura, V., do Socorro Monteiro Leal, L., Botia, S., Lavrič, J.,
1342 Komiya, S., Frumau, A., Hensen, A., van den Bulk, P., van Dinter, D., and Notholt, J.:
1343 Tropical forest CH₄: from flux chambers to micrometeorological tower measurements,
1344 EGU General Assembly 2020, Online, 4–8 May 2020, EGU2020-6139,
1345 <https://doi.org/10.5194/egusphere-egu2020-6139>, 2020.

1346 Vella, R., Forrest, M., Pozzer, A., Tsimpidi, A. P., Hickler, T., Lelieveld, J., and Tost, H.:
1347 Influence of land cover change on atmospheric organic gases, aerosols, and radiative
1348 effects, *Atmos. Chem. Phys.*, 25, 243–262, <https://doi.org/10.5194/acp-25-243-2025>, 2025.

1349 Venturini, A. M., Gontijo, J. B., Mandro, J. A., Berenguer, E., Peay, K. G., Tsai, S. M., and
1350 Bohannan, B. J. M.: Soil microbes under threat in the Amazon rainforest, *Trends Ecol.*
1351 *Evol.*, 38, 693–696, <https://doi.org/10.1016/j.tree.2023.04.014>, 2023

1352 Wang, H., Liu, X., Wu, C., and Lin, G.: Regional to global distributions, trends, and drivers
1353 of biogenic volatile organic compound emission from 2001 to 2020, *Atmos. Chem. Phys.*,
1354 24, 3309–3328, <https://doi.org/10.5194/acp-24-3309-2024>, 2024.

1355 Wang, M., Zheng, Q., Shen, Q., and Guo, S.: The critical role of potassium in plant stress
1356 response, *Int. J. Mol. Sci.*, 14, 7370–7390, <https://doi.org/10.3390/ijms14047370>, 2013.

1357 Warneke, C., Veres, P., Murphy, S. M., Soltis, J., Field, R. A., Graus, M. G., Koss, A., Li,
1358 S. M., Li, R., Yuan, B., Roberts, J. M., and de Gouw, J. A.: PTR-QMS versus PTR-TOF
1359 comparison in a region with oil and natural gas extraction industry in the Uintah Basin in
1360 2013, *Atmos. Meas. Tech.*, 8, 411–420, <https://doi.org/10.5194/amt-8-411->, 2015.

1361 Wells, K. C., Millet, D. B., Payne, V. H., Vigouroux, C., Aquino, C. A. B., De Mazière, M.,

1362 de Gouw, J. A., Graus, M., Kurosu, T., Warneke, C., and Wisthaler, A.: Next-generation
1363 isoprene measurements from space: detecting daily variability at high resolution, J.
1364 Geophys. Res. Atmos., 127, e2021JD036181, <https://doi.org/10.1029/2021JD036181>, 2022

1365 Yáñez-Serrano, A. M., Nölscher, A. C., Bourtsoukidis, E., Gomes Alves, E., Ganzeveld, L.,
1366 Bonn, B., Wolff, S., Sa, M., Yamasoe, M., Williams, J., Andreae, M. O., and Kesselmeier,
1367 J.: Monoterpene chemical speciation in a tropical rainforest: variation with season, height,
1368 and time of day at the Amazon Tall Tower Observatory (ATTO), Atmos. Chem. Phys., 18,
1369 3403–3418, <https://doi.org/10.5194/acp-18-3403-2018>, 2018.

1370 Yáñez-Serrano, A. M., Bourtsoukidis, E., Alves, E. G., Bauwens, M., Stavrou, T., Llusà,
1371 J., Filella, I., Guenther, A., Williams, J., Artaxo, P., Sindelarova, K., Doubalova, J.,
1372 Kesselmeier, J., & Peñuelas, J. Amazonian biogenic volatile organic compounds under
1373 global change. Global Change Biology, 26(9), 4722-4751.
1374 <https://doi.org/10.1111/gcb.15185>, 2020.

1375 Yáñez-Serrano, A. M., Filella, I., Llusà, J., Gargallo-Garriga, A., Granda, V.,
1376 Bourtsoukidis, E., Peñuelas, J., et al.: GLOVOCS-master compound assignment guide for
1377 proton transfer reaction mass spectrometry users, Atmos. Environ., 244, 117929,
1378 <https://doi.org/10.1016/j.atmosenv.2020.117929>, 2021

1379 Zannoni, N., Leppla, D., Lembo Silveira de Assis, P. I., et al.: Surprising chiral composition
1380 changes over the Amazon rainforest with height, time and season, Commun. Earth Environ.,
1381 1, 4, <https://doi.org/10.1038/s43247-020-0007-9>, 2020

1382 Zannoni, N., Wikelski, M., Gagliardo, A., et al.: Identifying volatile organic compounds
1383 used for olfactory navigation by homing pigeons, Sci. Rep., 10, 15879,
1384 <https://doi.org/10.1038/s41598-020-72525-2>, 2020.

1385